Received: 30 January 2022 | Revised: 21 July 2022 | Accepted: 5 August 2022

DOI: 10.1002/idm2.12058

REVIEW

Interdisciplinary Materials — Open Access WILEY

Structural-functional unit ordering for high-performance electron-correlated materials

Guyang Peng[1] | **Lei Hu**[1] | **Wanbo Qu**[1] | **Chenglong Zhang**[1] | **Shurong Li**[1] | **Ziyu Liu**[1] | **Juncheng Liu**[1] | **Shengwu Guo**[1] | **Yu Xiao**[1] | **Zhibing Gao**[1] | **Zhen Zhang**[1] | **Yang Zhang**[2] | **Haijun Wu**[1,2] | **Stephen J. Pennycook**[1,2,3] | **Jun Sun**[1] | **Xiangdong Ding**[1]

[1]State Key Laboratory for Mechanical Behavior of Materials, Xi'an Jiaotong University, Xi'an, China

[2]Instrumental Analysis Center, Xi'an Jiaotong University, Xi'an, China

[3]Department of Materials Science and Engineering, University of Tennessee, Knoxville, Tennessee, USA

Correspondence
Haijun Wu, Stephen J. Pennycook, and Xiangdong Ding, State Key Laboratory for Mechanical Behavior of Materials, Xi'an Jiaotong University, Xi'an 710049, China.
Email: wuhaijunnavy@xjtu.edu.cn, stevepennycook@gmail.com and dingxd@xjtu.edu.cn

Abstract

Electron-correlated materials have been drawing ever-increasing attention due to their fascinating physical behaviors and extensive application scenarios. In this review, a new method for material research and design (R&D), named structural-functional unit ordering (SFU ordering), which is presented, overcomes the shortcomings—for example, the limitation of finite chemical elements and long R&D circle-of conventional strategy and thus provides guidance for the design of these high-performance functional materials on demand. Meanwhile, with the development of material characterization technologies, SFUs of different scales and types can be directly observed, which, moreover, regulate the corresponding orderings. The review, starts with an introduction of the profile for SFU ordering and the synergistic effect between SFUs. Then, studies on several new high-performance electronic-correlated materials, for example, a ferromagnetic semiconductor with local spin, ferromagnetic metals with spin topologies, ferroelectric thin films with polar topologies, piezoelectric thin films with nanopillars enclosed by charged boundaries, thermoelectric materials with local ferromagnetic nanoparticles and topotactic phase transformation with conducting nanofilaments are stated in detail one by one. The vital aspect is the breaking of local symmetry, the construction, the structure, of SFUs and their orderings existing or theoretically existing, together with the enhanced/new performance. All in all, the main comments of the review tend to the remaining challenges, promising design approaches for the SFUs, and their orderings for high-performance functional materials.

KEYWORDS

electron-correlated materials, ferroelectric, piezoelectric, structural-functional unit, thermoelectric

1 | INTRODUCTION

1.1 | Structural–functional units and ordering

Reductionism holds that complex systems, things, and phenomena can be understood and described as a combination of parts. The scientific research model based on reductionism has achieved glorious results, and its methodology is characterized by the research paradigm of "composition—structure—performance" in the field of material science. This research method based on composition and crystal structure from the periodic table of elements has spawned a series of material design methods such as material strength theories, solid physics, quantum mechanics, and so forth. However, the traditional material research and design (R&D) methods are limited by the finiteness of chemical elements and the long-time cycle. To shorten the R&D cycle and design new materials with better performance or new phenomena on demand without limitation, we need to change from the traditional strategy to a new material R&D method.[1]

In many cases, the behavior of large and complex basic-particle aggregates cannot be understood according to the simple extrapolation of a few basic particles, and the transformation process from quantitative change to qualitative change can be explained by the influence of some specific structures artificially designed and their orderings. Let's start from two-dimensional (2D) materials with emphasis on magic-angle graphene, a kind of star 2D material. Recently, Abhay N. Pasupathy et al. studied the structural characterization and electronic structure of the three-layer torsional graphene structure (TTG). It was found that the moiré lattice in the TTG would be reconstructed, thus forming a series of triangular regions and some special sites around them.[2] These artificial special structures had a significant impact on atomic periodicity and electronic structure, and these structures could directly relate to the brand-new performance of the material. In this case, the triangular regions and the surrounding sites are the structural units designed and manufactured manually with specific functions for materials, which we call SFU in this review. Obviously, the arrangement of these structural units is directly related to different moiré lattices and therefore to the macroscopic performance, which we call the ordering of SFU. In addition to twisted 2D materials, in the process of vertical stacking to form vertical van der Waals heterostructures or mixed stacking (e.g., stacking 2D materials with other dimensional materials), various SFUs and SFU orderings will be constructed.[3] Based on this idea, the research paradigm of "composition-structure-performance" could be transformed into a new paradigm of "SFU—SFU ordering—performance." It is worth noting that the focus of the division of SFU should not be its size but whether the SFUs and their orderings are coupled to trigger the new performance of material emergence, and the incisive dimension we select should be based on the level of key research objects. SFUs intersect with some conventional structural concepts such as domains, grains, interfaces, and so forth. For instance, domain boundaries are important SFUs in a variety of functional materials. The local symmetry breaking caused by the special homo-interfaces in ferroelectrics can introduce novel phenomena such as local metallic conductivity or magnetism. However, the difference is that a considerable part of SFUs do not exist naturally, which indicates that we can flexibly design efficient special structures for a certain functional system. In addition, most of SFUs are realistic structure units that can be directly characterized. However, few SFUs, such as skyrmions, behave as quasiparticle, for example, a phenomenon rather than a really independent object. These special SFUs are often controlled by multiple coupling factors so their observation and regulation are quite difficult, remaining further research. When we come to the ordering, the key lies in the specific synergistic correlation effect of it, that is, the arrangement mode, such as ordered/disordered distribution, geometric arrangement, size of SFU, and so forth, which can change the intrinsic properties of materials compared with disorderedly distributed units. More specifically, the performance presented by SFU+ ordering will exceed that of SFU itself. Besides the 2D material systems mentioned above, the idea of SFU ordering has been applied in the field of optics and photonics, so-called metamaterials, covering photonics circuits, sub-diffraction-limited optical imaging, environmental and health-care sensing,[4] and so forth. This strategy then extended the idea of SFU ordering to other wave systems (such as acoustics), based on which the next generation of acoustic technologies, for example, zero/negative refraction, subwavelength imaging, sound cloaking, meta-surface, and so forth.[5] has been greatly developed. It is also possible to control heat conduction and is expected to be applied to modern core technologies, for example, microelectronics and aerospace.[6] The SFU ordering strategy not only bends the fundamental rules of light (even waves) in optics,[7] but also plays an essential role in Schwarz metals,[8] ceramic-based dielectric metamaterials,[9] electrochemical capacitances with 2D quantum-sheet films[10]

and nanoscale 3D architecture,[11] catalysts with atomic clusters and nanoparticles,[12] batteries with 3D ion channels,[13] and so forth. We are wondering whether it can create new miracles in broader fields.

1.2 | Electron-correlated materials

This review attempts to popularize the new research paradigm of "SFU—SFU ordering—performance" to explore new efficient electron-correlated materials. As the "precursor" of quantum materials, electron-correlated materials are not limited to strong electron-correlated materials such as magnetic materials. Actually, most of the objects of modern condensed state physics and functional material science can be included in the category of electron-correlated materials. From the perspective of the macroscopic properties of materials, it is shown that the electrical response can act as an intermediary, making the force, heat, magnetism, and other forms of energy related, as shown in Figure 1. From the aspect of degrees of freedom, the medium, and charge, could directly or indirectly correlate with lattice, spin, orbit, and so forth, to form various coupling effects for functional materials, as shown in Figure 1.

Magnetoelectrics with the spin and charge coupling,[14] ferroelectrics/piezoelectrics with the polarization charge and lattice strain coupling,[15] the thermoelectrics with the carrier and phonon coupling,[16] and resistive switching topological materials with the carrier and orbit coupling[17] could be considered as representative electron-correlated materials. Once considering SFU, all electronic features of these materials, for example, band structure, carrier/phonon transport behavior, lattice distortion/vibration, and spin electron/orbit coupling could be dramatically changed and influence macro performance. When we further consider the ordering of SFUs, in many cases the impact of SFUs will be deepened, sometimes even a brand-new phenomenon could be generated due to the synergistic correlation effect. Although in some material systems, there has been no specific experimental result support for the regulation of SFU ordering, this review would propose a potential design direction in these fields. Figure 2 summarizes these electron-correlated materials with their SFU, SFU ordering, enhanced/new properties, and application prospects. From the point of view of material

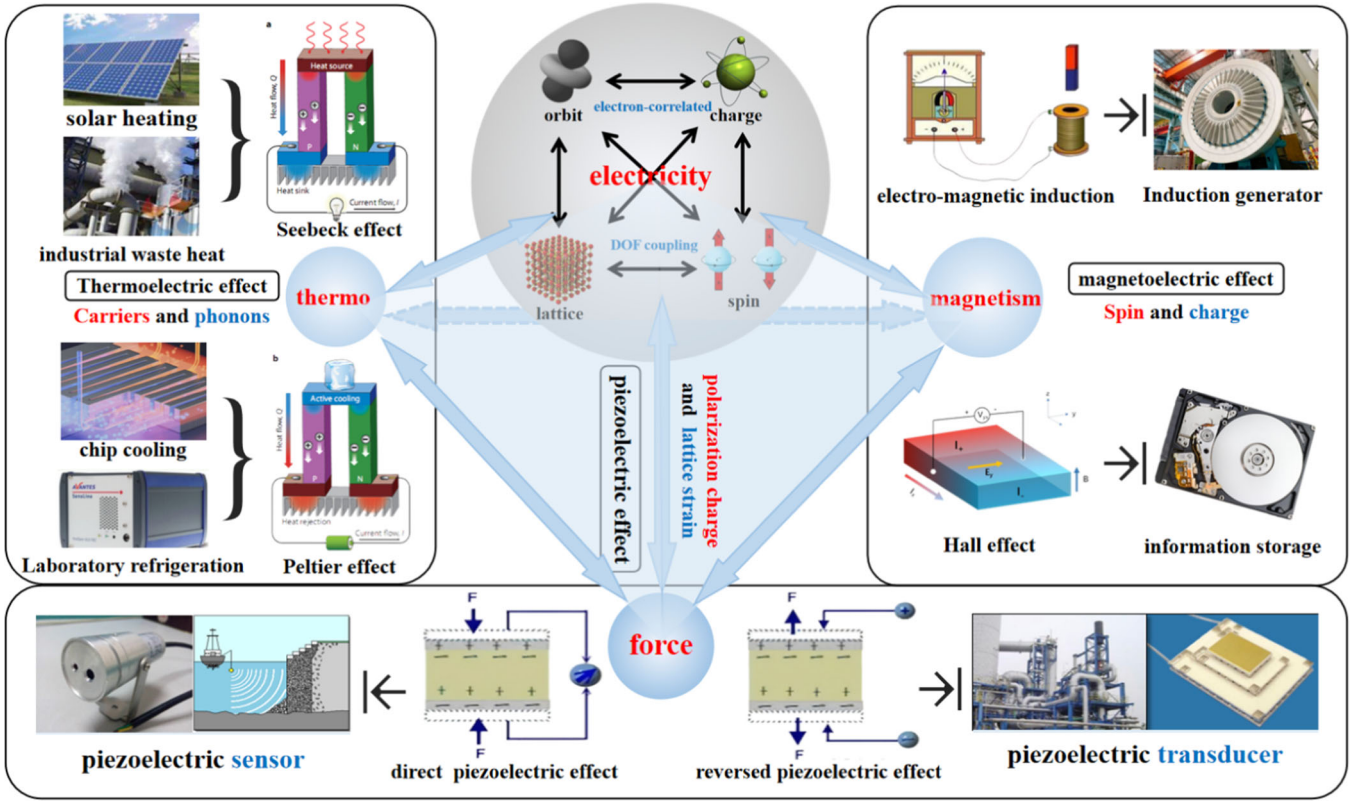

FIGURE 1 Electron-correlated materials: Coupling effects from the aspect of degrees of freedom and applications

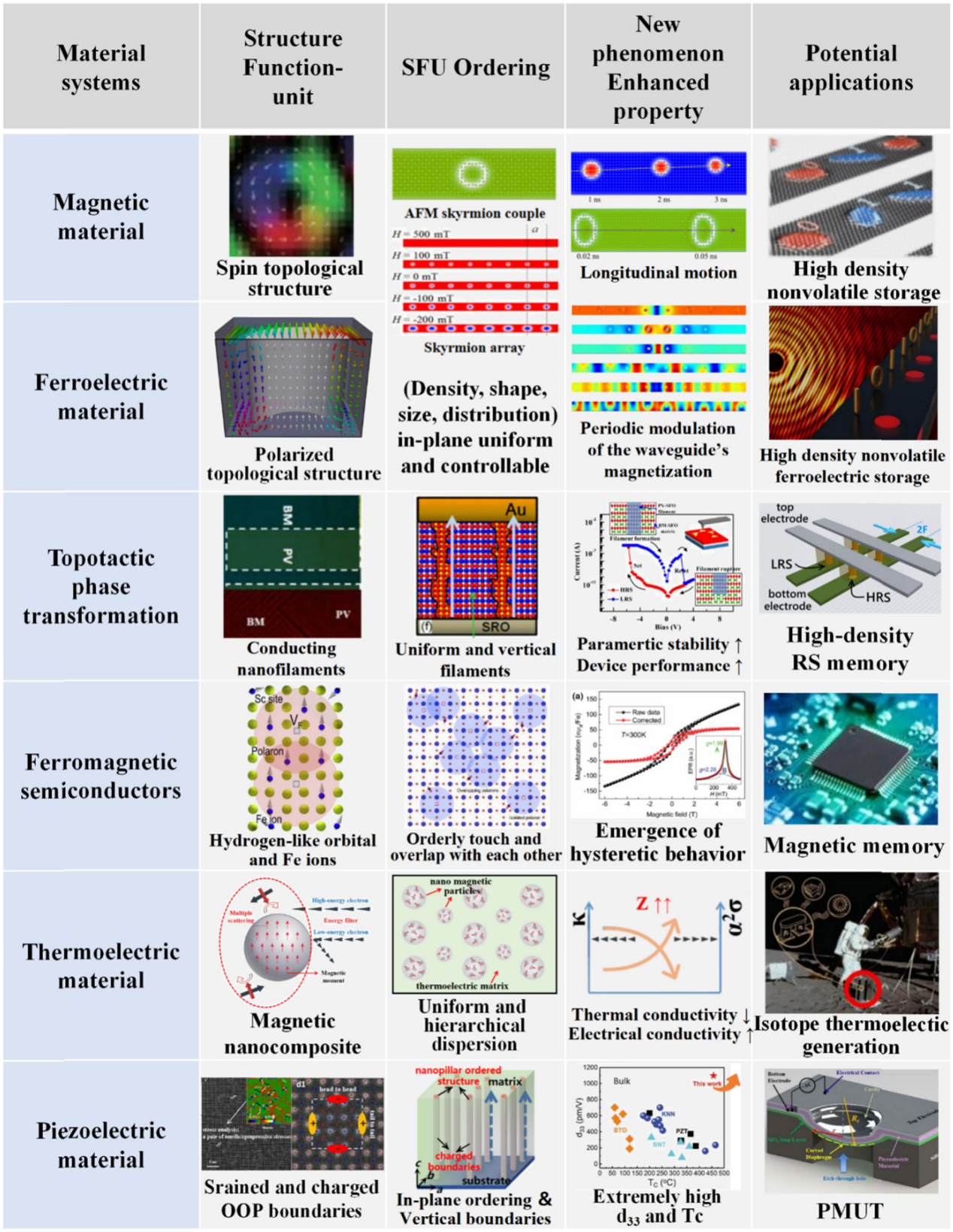

FIGURE 2 Summary of several types of electron-correlated materials with their SFUs, SFU ordering, enhanced/new properties, and application prospects. SFU, structural-functional unit.

engineering, this paper will focus on several methods on how to construct SFUs, such as point defect engineering and stress engineering, the findings should make an important contribution to the needs of designing high-performance SFU materials on demand. This review provides insights into a special class of SFUs, namely the local symmetry breaking SFUs, which construct a long-range high symmetry matrix and short-range low symmetry nanoregions within it. For the order parameters with long-range properties such as ferromagnetism and ferroelectricity, this local symmetry breaking will cause the local short-range of the order parameters, thus improving the dynamic response of the material.

Through a brief review of the above examples, we have preliminarily demonstrated the studies of electron-correlated materials from the perspective of SFU ordering. The following main text would demonstrate one example for each type of electron-correlated materials in detail, following the scenario from how to construct, how to evidence the SFUs and their orderings, and how to correlate them with enhanced property or new phenomenon.

2 | MAIN BODY

2.1 | Ferromagnetic semiconductors: Hydrogen-like orbital and surrounding Fe ions as SFUs for spin electronics

The first case of electron-correlated materials based on SFU ordering is local spin orders of ferromagnetic semiconductors for spin electronics. If the electronic-spin properties in magnetic materials could be combined with the electronic-charge properties in semiconductor materials, the electric field can be used to control the charge and spin simultaneously to realize the separation of computing and storage functions. Such a coupling effect could greatly improve the speed of reading and writing of chips. To obtain semiconductors with intrinsic magnetism, magnetic atoms can be doped into semiconductor materials. For example, Mn was doped into PbSnTe and InAs, to obtain magnetic-doped semiconductor systems,[18] whose anomalous quantum Hall effect regulated by electric field creates an interesting area of magnetic semiconductor materials. However, up to now, the temperature stability of magnetic semiconductor materials is still poor, which limits its practical application.

Hu et al. did not introduce magnetic elements, instead used the method of the anion-induced magnetic dipole to avoid the clusters of magnetic impurities.[19] The $(SC_{1-x}Fe_x)F_3$ samples have been prepared by solid-state synthesis method and the short-range low symmetric Fe-F ferromagnetic ordered phase as SFU distribute in the long-range highly symmetric ScF_3 matrix, realizing the coupling of charge and spin degrees of freedom, and the obtained magnetic semiconductor materials have high-temperature stability ($T_c \sim 545$ K). Here the high-temperature magnetic order formed in ScF3-based solids provides an intriguing instance.[19a] ScF_3 demonstrates diamagnetism due to the $3d^0$ electronic configuration of Sc^{3+}. Surprisingly, high-temperature ferromagnetism is found in its ion-doped ScF_3. SFU ordering plays a critical role in the formation of local spin order. At first, ScF_3 crystallizes into the cubic structure with the space group of $Pm\text{-}3m$. Sc is sixfold coordinated with fluorine atoms to form ScF_6 octahedra, as demonstrated in Figure 3A. With the introduction of Fe into the ScF_3 host matrix, the Fe atom also occupies the crystallographic site of Sc in $(Sc,Fe)F_3$ solid solutions. In $(Sc,Fe)F_3$ solid solution, the intrinsic fluorine defects, especially fluorine vacancies, V_F, revealed as black boxes in Figure 3B, tend to act the donors and demonstrate positive charge centers, which capture localized electrons and generate hydrogen-like orbitals, shown by the red circle in Figure 3B. The electron captured by the V_F interacts with electrons residing in Fe 3*d* orbitals, shown by blue spheres with arrows. This structure, involving the localized electron and Fe ions, consists of the unique SFU, among which a certain interaction effect enables the alignment of spins of Fe 3*d* electrons. This peculiar SFU is demonstrated by the red circle in Figure 3B. When the concentration of V_F reaches the critical point, these peculiar SFUs are inclined to touch and furthermore overlap with each other. This organization occurs in one-dimensional 1D, 2D or 3D scales, which drives the magnetic moments lining up, so-called SFU ordering. With further removing V_F by chemical modifications, there are no existing positive charge centers, and no electrons would be captured to form this uncommon SFU. Consequently, there is lacking interaction among Fe 3*d* electron spins, which tend to align randomly. Consequently, ferromagnetism is switched off. This scenario is depicted in the right panel of Figure 3B. Neutron powder diffraction (NPD) performed in $(Sc,Fe)F_3$ does not show superstructure peaks from long-range magnetic structure, as shown in Figure 3C. This is strong evidence to confirm the short-range magnetic structure. As revealed in Figure 3D, Near-edge X-ray absorption fine structure (XAFS) spectra show the location of Fe K edge of $(Sc,Fe)F_3$ samples treated under different atmospheres higher than the Fe^{2+} K edge and lower than the Fe^{3+} K edge. These experimental results reveal the mixed chemical valence of Fe in $(Sc,Fe)F_3$ and also the existence of V_F. The simulated and experimental radical distribution function in Figure 3E of $(Sc,Fe)F_3$ samples demonstrate similar coordination peaks, confirming the occupancy of

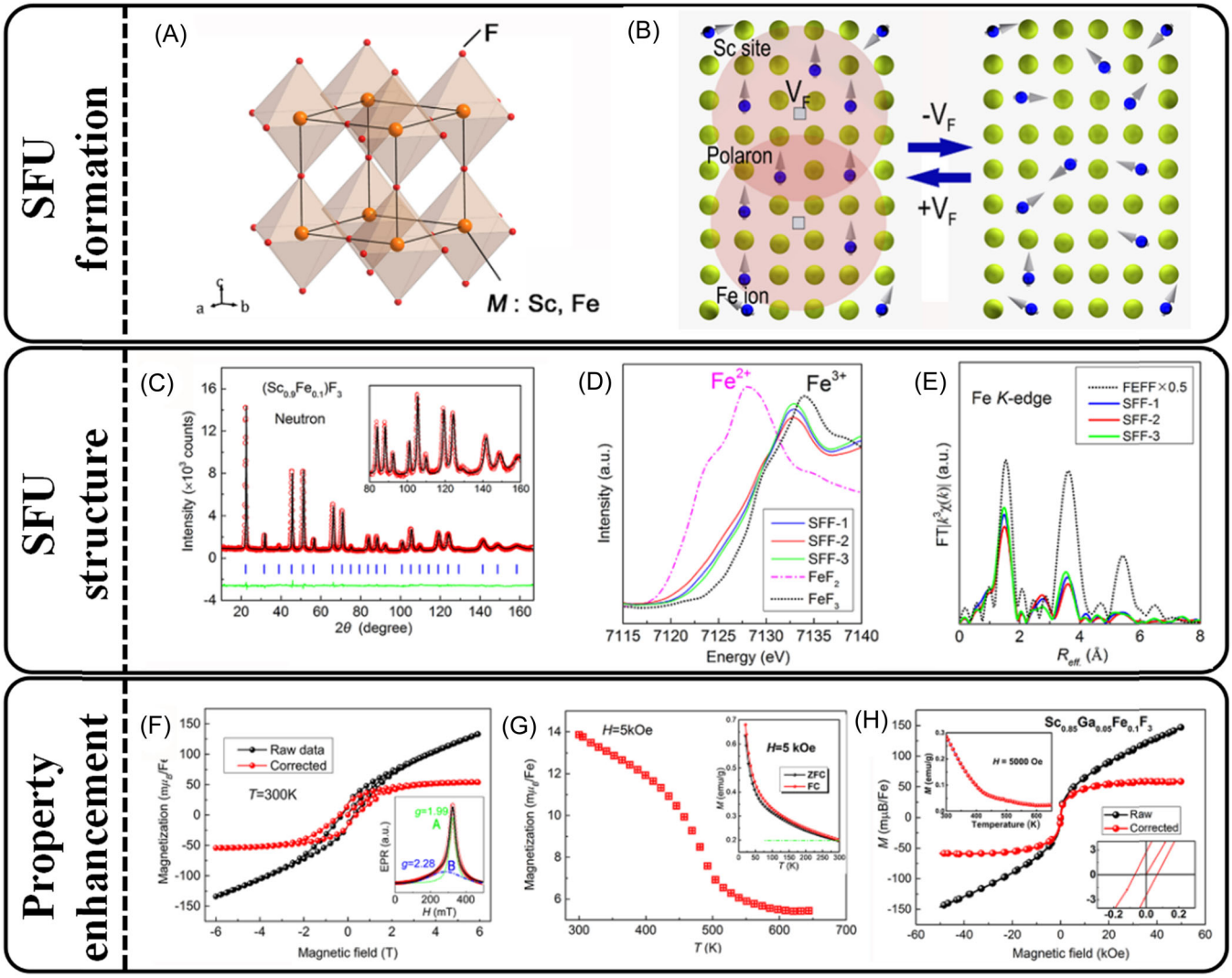

FIGURE 3 Ferromagnetic semiconductors with local spin orders as SFU ordering. (A) Crystal structure of $(Sc,Fe)F_3$. (B) The formation of SFU, consisting of the hydrogen-like orbital (red circle) and Fe ions (blue spheres with arrows). This unit is triggered by the fluorine vacancy, V_F. (C) Neutron powder diffraction of $(Sc,Fe)F_3$. (D) Near-edge x-ray absorption fine structure spectroscopy (XAFS) of $(Sc,Fe)F_3$ with standard samples, FeF_2 and FeF_3. (E) Simulated and experimental Fourier transformation of Fe K-edge XAFS of different $(Sc,Fe)F_3$ samples. (F) Magnetic hysteresis loop (*M-H*) of $(Sc,Fe)F_3$. The inset shows the electron paramagnetism resonance spectroscopy (EPR). (G) Temperature dependence of magnetism of $(Sc,Fe)F_3$. The inset indicates the *M-T* curves under zero-field cooling and field cooling conditions. (H) *M-H* curves of $(Sc,Ga,Fe)F_3$. The insets demonstrate the *M-T* curve and the zoomed region at the low magnetic field. (C–G) Reproduced with permission from Hu et al.,[19a] copyright 2015 Wiley. (h) Reproduced with permission from Hu et al.,[19b] copyright 2014 American Chemical Society. SFU, structural-functional unit.

Fe at Sc site even in the local region. This peculiar SFU ordering found in $(Sc,Fe)F_3$ generates robust and soft ferromagnetism as shown in Figure 3F. The inset shows the electron paramagnetic resonance (EPR) spectrum, consisting of two components A and B. Component A indicates the randomly distributed spins of 3*d* electrons in Fe ions. Significantly, component B confirms the existence of aligned 3*d* electrons in $(Sc,Fe)F_3$, which supports the physical scenario of SFU ordering depicted in Figure 3B. Furthermore, the ferromagnetism could resist strong thermal fluctuation and enable the Curie temperature (T_c) up to ~545 K,[19a] as shown in Figure 3G. In addition, this peculiar SFU ordering is also found in $(Sc,Ga,Fe)F_3$ system, which also gives rise to interesting ferromagnetism and high T_c up to ~435K,[19b] as shown in Figure 3H. The bottom-right inset indicates the small coercive field of several hundred Oe.

The introduction of Fe-F SFUs in ScF_3 induces magnetism, which overcomes the great obstacle of lattice and chemical bonding between magnetic elements and nonmagnetic semiconductors, and avoids the precipitation of

magnetic precipitates from the semiconductor matrix. Besides the trade-off between semi-conductivity and magnetism, there are many order parameters that are difficult to be coupled in various material systems. For instance, ferroelectricity versus semi-conductivity, ferromagnetism-electricity, ferroelectricity versus ferromagnetism, and topology versus ferroelectricity are to be described below. To solve these reciprocal relations, some special structures can be artificially designed and introduced to control the gradient of the order parameters in the spatial distribution, so that the mutually exclusive functions could be weakened dramatically and thus new coupling could be achieved. For example, the charged interfaces in ferroelectrics form a local symmetry breaking, which makes the band and polarization exhibit a spatial gradient at the interfaces, so that the intrinsically insulated ferroelectrics exhibit local semi-conductivity and even metallic conductivity.[20] It can be seen that the SFU itself can act as a device, and more importantly, its topological structure can introduce intrinsically non-existent or even contradictory properties in uniform materials.

2.2 | Ferromagnetic metals: Spin topologies as SFUs for high-density memories

The second case of electron-correlated materials based on SFU ordering is spin topological ferromagnetic materials for high-density magnetic storage. Although the application of giant magnetoresistance (GMR) and spin transfer torque magnetic random-access memory (STT-MRAM) technologies have made great progress in magnetic storage in terms of storage speed, energy consumption, and heat generation, the core principle of traditional magnetic storage is still to use magnetic domain inversion to read and write, resulting in huge Joule heat and high energy consumption, hindering the further development of magnetic storage. Ferromagnetic topological structure, as the studied SFU, appears at the atomic scale as an ordered arrangement similar to the lattice at the scale beyond the lattice. Because its ability to store information and its driving current is much less than that of flipping the magnetic domain wall, the application of magnetic topological sequences such as vortex,[21] skyrmions,[22] and merons[23] in magnetic storage is expected to achieve high-density data reading and writing. This review will focus on the topological structure of magnetic skyrmions as an example, which is a promising non-volatile storage carrier with ultra-small size, high stability, and controllable characteristics, and is not easy to be pinned during movement, for example, topological protection. The magnetic topological SFU can be regarded as a large special structure formed by the ordered assembly of magnetic dipoles. Different ordered assembles present varied morphologies of SFU and cause different responses to the external field.

The skyrmion is a nanoscale magnetic vortex structure, in which the spin points to all directions around the sphere, as schematically shown in Figure 4B1,B2. The common strategy is to finely manipulate temperature, such as driven by thermal fluctuation near the critical conditions and applied magnetic field to construct a metastable magnetic skyrmion phase, driven by thermal fluctuation near the critical condition. The skyrmion state exists only in a small region of the phase diagram, as shown in Figure 4A. The magnetic skyrmion was proposed in 2006,[24] and experimentally detected in MnSi single crystal in 2009 using neutron scattering[22d] (Figure 5).

In 2010, X. Z. Yu grew the $Fe_{0.5}Co_{0.5}Si$ single crystal using the floating-zone technique and the crystal quality was checked by powder X-ray diffraction and energy-dispersive X-ray spectroscopy. Then they directly observed the skyrmions in the thin film by combining the real-space observation by Lorentz transmission electron microscope (TEM) and theoretical calculation based on two-dimensional spin model of DM interaction and anisotropy.[22c] Under the magnetic field of 50 mT, the structure is spin fringes at 5 K while hexagonal ordered magnetic skyrmions at 25 K, as shown in Figure 4C1,C2. At 25 K below the magnetic transition temperature (40 K), the magnetic domain structure presents orderly spin fringes under the zero-field state, while changes to ordered hexagonal skyrmions under the magnetic field of 50 mT, as shown in Figure 4D1,D2. The results verify that both temperature field and magnetic field have a great influence on the formation of skyrmions. In Figure 4F,G, the phase change of the spin texture is represented as a contour map of the skyrmion density. The experimental and theoretical results congruously reveal not only the phase transition behavior between the helical state and skyrmion state but also the transition coexistence region between them. The spin skyrmion state seems to be stable and appears in a wide range of the phase diagram, including temperatures close to zero.

Spin topologies in magnetic materials, especially spin skyrmions, have attracted extensive attention. With the help of Lorentz TEM, it is possible to evaluate the topological factors of spin configuration and magnetic domain structure by directly observing spin configurations and magnetic domains. Based on the in-depth study of the relationship between the topological magnetic structure and magnetic properties of magnetic materials, new materials with novel and adjustable spin topologies can be achieved, which induce various new applications.

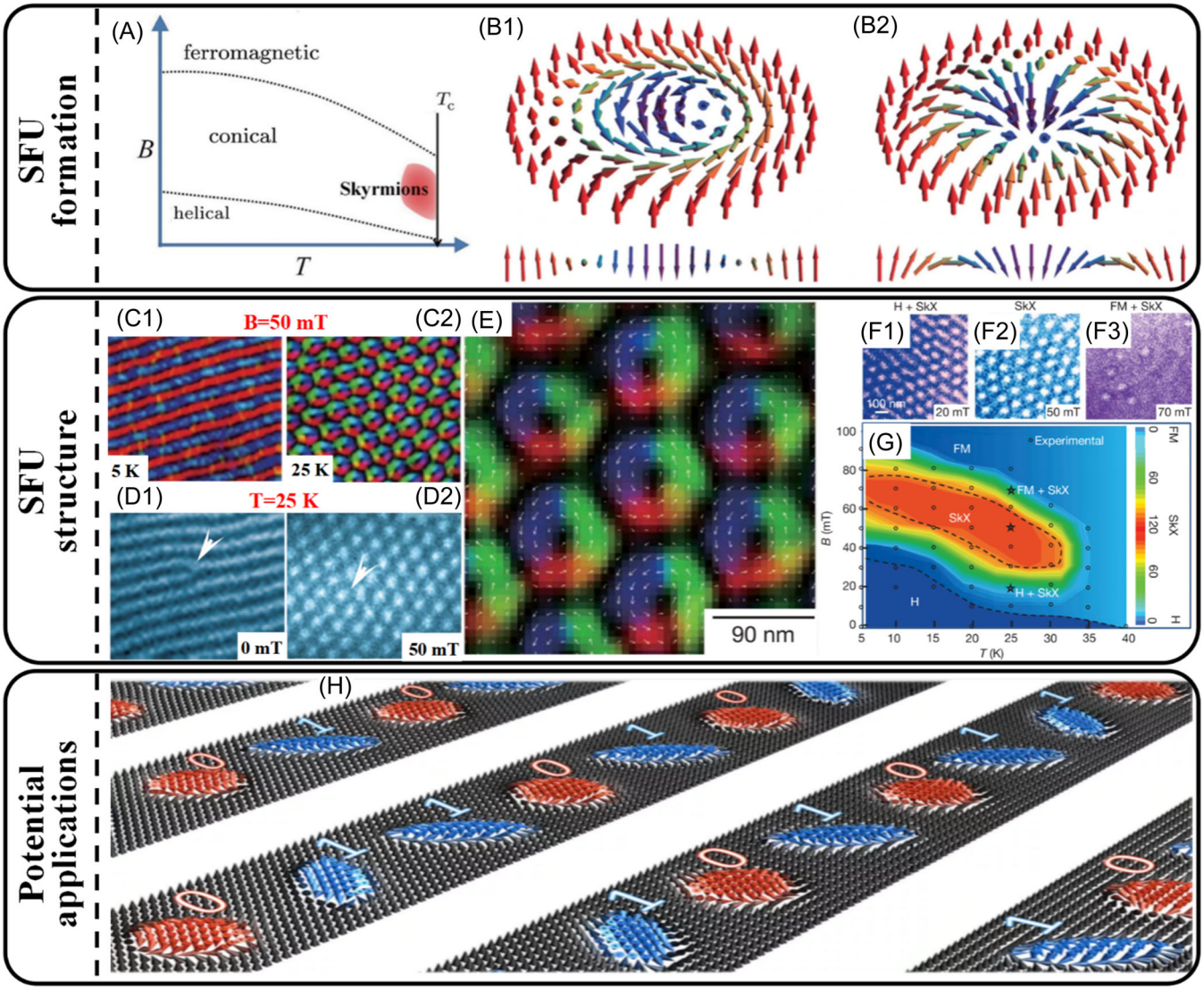

FIGURE 4 SFU in ferromagnetic, spin, for high-density magnetic memories. (A) The phase diagram of magnetic structure in bulk helical magnets showing skyrmion forms only in a narrow region below T_c. (B1, B2) Two forms of skyrmions: Bloch Type and Neel type. (C, D) Topological spin textures in the helical magnet. (C1, C2) Temperature profiles of the distribution map of the lateral magnetization for a magnetic field of 50 mT. Magnetic fields were applied normal to the (001) thin film. The color wheel represents the magnetization direction at every point. (D1, D2) Magnetic domain structure without magnetic field and 50 mT perpendicular to thin film. (F1, F2, F3) Spin textures observed using Lorentz TEM obtained by Monte Carlo simulation. H, helical structure. (G) Observation phase diagram on B–T plane. (H) Schematics showing magnetic skyrmions as information carriers for magnetic storage schemes, where 0/1 states are marked with different topological features. (C–G) Reproduced with permission from Yu et al.,[22c] copyright 2010 Springer Nature. SFU, structural-functional unit; TEM, transmission electron microscope.

There are three basic processes for skyrmion-based information storage and processing, that is, writing (nucleation of individual skyrmions), processing (displacement of skyrmions), and reading (detection of skyrmions). Hence, the prerequisite for the use of skyrmions in devices is the ability to stabilize ultra-small individual skyrmions at room temperature, together with zero or very small applied fields. Through the interaction between multi-layer films and the preparation of materials such as magnetron sputtering, the stable existence of skyrmions at room temperature and the low magnetic field have been obtained. To obtain an individual unit rather than a lattice, the effective DMI constant between layers should be tuned. Therefore, in the dimension of structure, the ordering regulation of skyrmions is mainly in its size regulation. Obviously, the smaller size of the skyrmions is, the larger the theoretical information storage density is. However, the size of the experimental results is usually more than 100 nm and there is an obvious size dispersion, which is mainly due

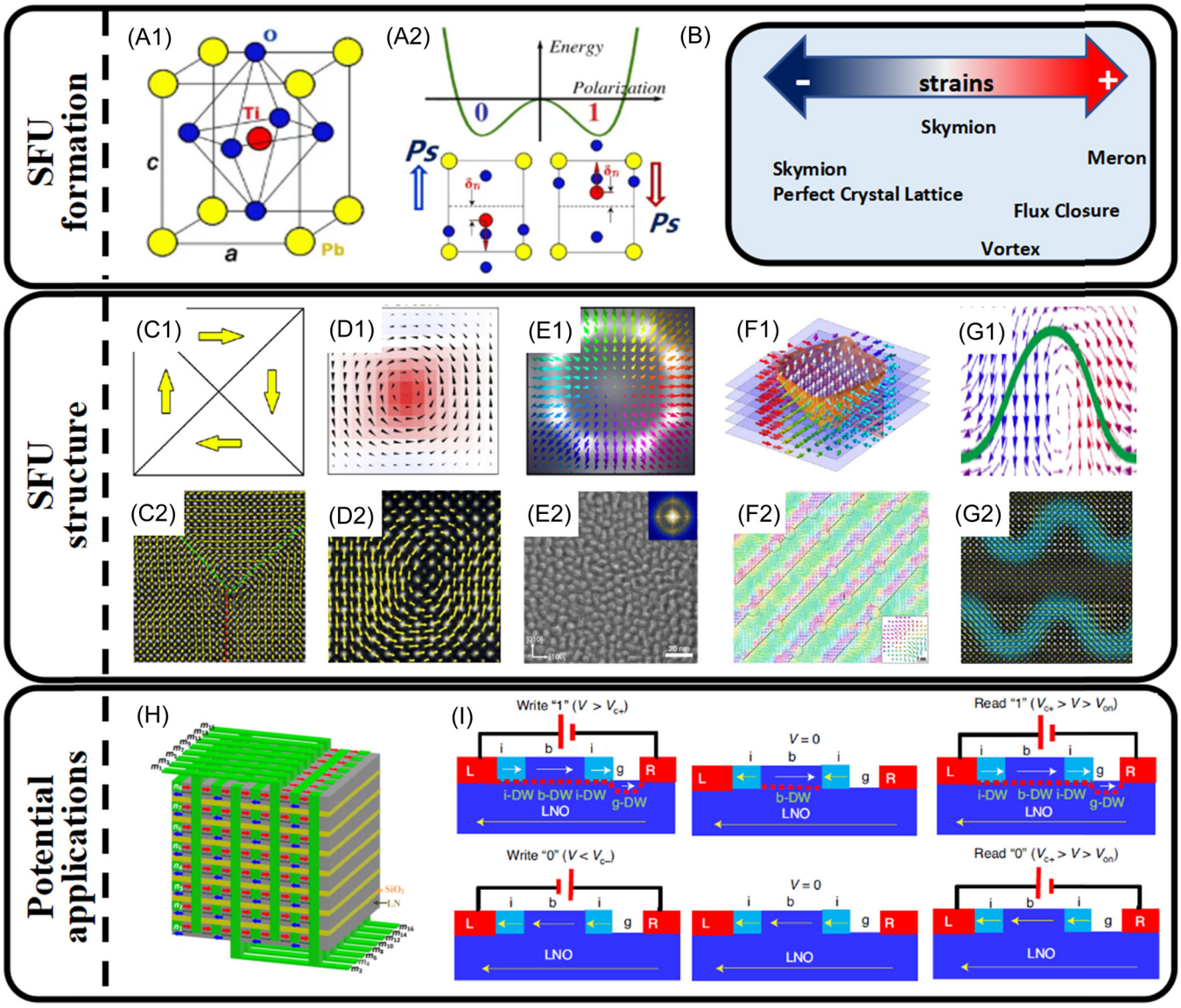

FIGURE 5 Polar topological structure as SFU in ferroelectric thin films. (A1, A2) Schematic diagram of lattice structure and polarization formation in perovskite. (B) Experimental relationship between external stress condition and existence of various polar topological structure. (C1, C2) (D1, D2) (E1, E2) (F1, F2) (G1, G2) Schematic and microscope observation of identified polar topological structures in a ferroelectric thin film, flux-closure, vortex, skyrmions, meron, and polar wave. (H, I) Schematic figure showing ferroelectric domain wall memory with embedded selector, and its wall creation/erasure under write and read operations, as a potential application in the high-density memory device. (A1, A2, C1, C2) Reproduced with permission from Tang et al.,[25b] copyright 2015 The American Association for the Advancement of Science. (B) Reproduced with permission from Wang et al.,[26] copyright 2021 American Institute of Physics. (D1, D2) Reproduced with permission from Yadav et al.,[27b] copyright 2016 Springer Nature. (E1, E2) Reproduced with permission from Das et al.,[28] copyright 2019 Springer Nature. (F1, F2) Reproduced with permission from Wang et al.,[26] copyright 2020 Springer Nature. (G1, G2) Reproduced with permission from Gong et al.,[29] copyright 2021 The American Association for the Advancement of Science. (H) Reproduced with permission from Jiang et al.,[30] copyright 2020 Springer Nature. SFU, structural-functional unit.

to the complex parameters that affect the size, making it difficult to control. The size of skyrmions is also closely related to their transport performance, such as velocity, but the specific impact is not clear, which is worthy of further study.[31]

In addition to the ordering regulation of a single skyrmion, it can also be artificially coupled. When driven by the spin-polarized current, the typical motion feature of a skyrmion in race tracks is the coexistence of a longitudinal motion and a transverse motion generated by gyrotropic forces, for example, the skyrmion Hall effect. The deflected motion would always annihilate the skyrmions at the edge of race tracks, which is unfavorable to any storage

technology. The antiferromagnetic skyrmions can be considered as two coupled topological spin configurations (skyrmion SFU) with opposite topological numbers due to the presence of antiferromagnetic exchange interaction. When the coupled skyrmions are driven by current, their opposite transverse deflections compensate, causing purely longitudinal motion.[32]

Magnonic crystals (MCs) are the magnetic analog of photonic and plasmonic crystals mentioned above with spatially periodic modulated magnetic properties. The periodicity of conventional MCs is structurally induced and static, but the ability to spatially control the nucleation of skyrmions indicates the creation of artificial periodic ordering of skyrmions in 1D or 2D nanostructure, for example, skyrmion-based dynamic magnonic crystal (SDMC). The advantage of the SDMC compared with the conventional MCs is the ability to dynamically reconfigure through (1) changing the diameter of the skyrmions by applying the applied field and the injected current; (2) manipulating the periodicity of the lattice by nanocontacts carrying a spin current.[33]

2.3 | Ferroelectric thin films: Polar topologies as SFUs for ultrahigh-density ferroelectric memories

The third case is the ferroelectric materials with polar topologies like the SFU. As mentioned above, the formation of special spin topologies in micro/nano ferromagnetic materials, as an important method to reduce magnetostatic energy, provides guidance for the design of storage cells and logic elements. In physics, topology aims to assemble real spatial order parameters into topological structures by controlling the degrees of freedom of spin, charge, orbit, and lattice. Ferroelectric materials are often studied by analogy with ferromagnetic materials because of their similar dipole structures. Corresponding to ferromagnetic spin topologies, ferroelectric polar topologies arises at the historic moment. Considering the anisotropy and spin rigidity of ferromagnets, the characteristic length scale of their internal spin topologies is generally in the range of several tens of nm to 100 nm, while ferroelectrics have higher anisotropy. If polar topologies can be kept at the same scale as the ferroelectric domain walls, that is, ~1/10 of the ferromagnetic domain walls, the ability to store and read information by switching/detecting the direction of polarization in ferroelectric materials will surpass conventional ferromagnetic materials. Therefore, it is possible to lead a new revolution of ultrahigh-density ferroelectric memory technology.

Lattice and charge are the main degrees of freedom of ferroelectric materials. By adjusting the balance between elastic energy, electrostatic energy, and polarization gradient energy, some polar topologies can stably exist in ferroelectric oxides. It can be envisaged that the applied electric field but not spin-polarized current is expected to effectively regulate the scale, density, stability, and other properties of such a new topological structure coupled with ferroelectricity. Compared with magnetic dipoles, the long-range nature of electric dipoles is much stronger, tending to parallel arrangement to form a long-range domain structure. The extremely large anisotropy energies or strain energy costs in rotating electric dipoles are the main obstacle to the construction of polar topologies in ferroelectrics.[34] Theoretical physicists employed the first principles to predict that the strong depolarization field generated by low-dimensional ferroelectric nanoparticles can stabilize the topological structure at the nanoscale.[35] To achieve a short-range local structure to form a topological configuration, a strong local depolarization field that is counter to the long-range ferroelectricity can be formed by introducing external strain. The required strain is derived from the local symmetry breaking caused by some other SFUs such as interfaces, nanodots, and localized composition heterogeneity, and so forth. In ferroelectric thin films, the applied strain field based on lattice mismatch can be introduced by precise thin-film epitaxial growth technology. For example, Tang et al. deposited n-$SrTiO_3$/n-$PbTiO_3$/n-$SrTiO_3$ three-layer films on STO substrate by RHEED-assisted pulsed laser deposition and observed the stable existence of skyrmions at room temperature, which reflects the advantages of thin films in generating polar topological structure compared with bulk materials. Strong coupling between strain and polarization in ferroelectric films is therefore becoming a core principle guiding the process of thin-film epitaxial growth controlling. Figure 6B demonstrates the experimental relationship between external strain conditions and the existence of various polar topological structures.[28] Besides, the introduction of nanodots will also form strain due to the high energy state of the surface, while it is difficult for bulk materials to introduce strain, local strain can be induced through deep doping or alloying.[38]

With the technological innovation of sub-angstrom electron microscopy such as spherical aberration-corrected scanning transmission electron microscope (STEM), atomic resolution imaging provides the ability to directly visualize electric dipoles and ferroelectric domain walls, and with subsequent

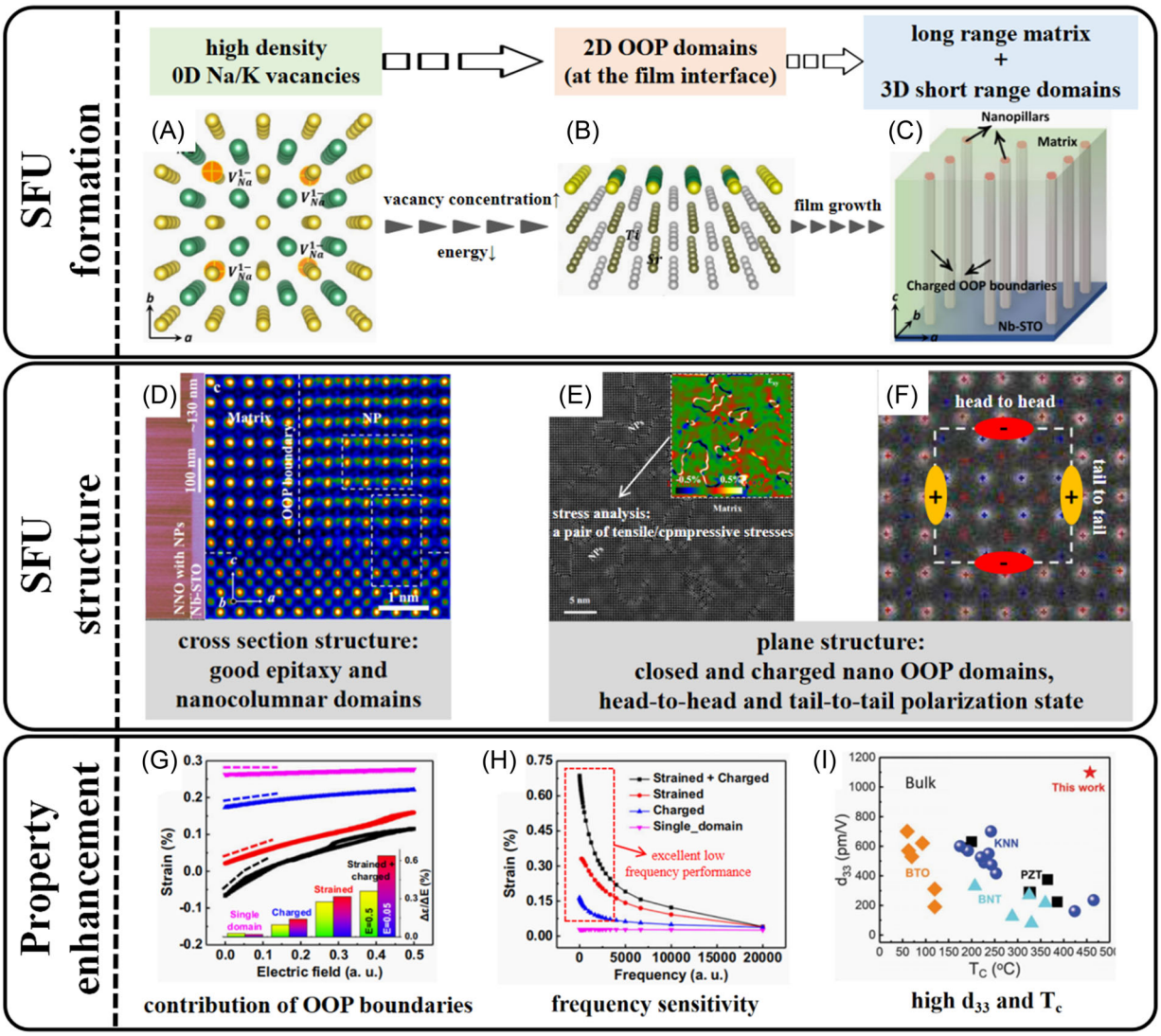

FIGURE 6 Nanopillar structure with 2D charged out-of-phase boundaries (SFU) in a piezoelectric thin film. (A) Atomic models showing 0D Na vacancies. (B) Atomic model showing the interface with 2D out-of-phase domain grown on the STO substrate for the first layer of the film. (C) Schematic for nanopillars with charged OOP boundaries embedded in the matrix. (D) STEM ABF image of the NP-NNO/STO film grown with a thickness of ~130 nm and atomically resolved STEM HAADF image showing one out-of-phase boundary and the NNO/STO interface. (E) High-magnification plan-view STEM HAADF image of NNO/STO showing a high density of nanopillars, with a strain analysis result inset. (F) Enlarged image of the regular nanopillar with 12 Nb atoms and polar nanopillar. (G) Average effective electric-field induced strain of single-domain NNO film for only strained, only charged, and charged + strained NNO films. The frequency is 10 a.u. The inset is the strain change over the electric field range of 0.05 and 0.5. (H) Average effective electric-field induced strain as a function of the frequency of the four cases in (G) with an applied electric field of 0.05 a.u. (I) Comparison of piezoelectric coefficient d_{33} of bulk material systems with this study (thin film) as a function of Curie temperature T_c. PZT, $Pb(Zr_{0.52}Ti_{0.48})O_3$-based piezoelectric materials; BTO, $BaTiO_3$-based piezoelectric materials; BNT, $(Bi_{0.5}Na_{0.5})TiO_3$-based piezoelectric materials; KNN, $(K_{0.5}Na_{0.5})NbO_3$-based piezoelectric materials. (A–H) Reproduced with permission from Wu et al.,[36] copyright 2021 Springer Nature. (I) Reproduced with permission from Liu et al.,[37] copyright 2020 Springer Nature. 2D, two dimensional; ABF, annular bright field; HAADF, high-angle annular dark field; SFU, structural-functional unit; STEM, scanning transmission electron microscope.

image processing and data analysis, directly characterize the polarization information is possible. In ferroelectric materials, various polarization topological structures have been observed including flux-closure structure (closure quadrants with closed head-tail dipole moments),[25] polar vortex domain (polarization revolves around a point to reduce the electric field),[27] polar skyrmion lattice (a quasiparticle-characteristic closing polarization unit protected by the topology),[28] polar meron lattice (half of a polar skyrmion),[26] polar wave structure (composed of electric dipoles connected at the head

and tail in a sine function form),[29] and so forth, as shown in Figure 6C–G.

At present, most of the frontier works on the polar topologies of ferroelectric thin films are carried out by the "iron triangle" of epitaxial parameter tuning, electron microscope observation, and calculation verification. The theory of interpretation is still immature and far from practical application. Although the direct control of polar topology structure is still a big challenge for high-density memories, its potential application range is wide-ranging. For example, the dynamic response of polar topology structure under the electric field, high energy electron beam or mechanical stimulation, namely the ability of external field coupled with phase transformation, will guide the design of the new mechanical, electrical and nonlinear optical-electronic devices. Moreover, the chiral polar topology has positive significance for the future development of controllable chiral devices and memory cells. Besides, topologically regulation of the number of ferroelectric domain walls in special polar structures could be promising to use in low energy cost and non-volatile memory devices, as shown in Figure 6H,I.[28]

2.4 | Piezoelectric thin films: Nanopillar structure with charged out-of-phase boundaries as SFUs for piezoelectric micromachined ultrasonic transducer

The fourth case of electron-correlated materials based on SFU ordering is a piezoelectric thin film with special nanoscale polar structures. The unique structures break the trade-off of piezoelectric properties, for example, the long-range property of ferroelectric polarization leads to the excellent static response (polarization intensity) but poor dynamic response (piezoelectric coefficient) of piezoelectric materials under the external field. Piezoelectric materials are widely applied for electromechanical sensors, actuators, and ultrasonic transducers.[39] For more than 60 years, $Pb(Zr,Ti)O_3$ (PZT) and $Pb(Mg_{1/3}Nb_{2/3})O_3$–$PbTiO_3$ (PMN–PT) with an excellent piezoelectric performance at the morphotropic phase boundary (MPB) has been "the material" for most piezoelectric devices.[40] However, its high toxicity and environmental unfriendliness are the main concerns, and it will soon be banned from use in many of the next-generation technologies. Therefore, there is an urgent need to develop lead-free counterparts.[39,41] The long-standing strategy to improve lead-free piezoelectric performance is to construct phase boundaries (similar to the MPB of PZT) through complex composition engineering. However, this strategy has intractable problems: (1) poor temperature stability due to greatly reduced Curie temperature and (2) poor reproducibility in manufacturing due to complex dopants of typically a few percent and involvement of high volatile elements.[37]

Wu et al. deposited different thicknesses of $NaNbO_3$ (NNO) films on (001) oriented 0.5% Nb-doped $SrTiO_3$ substrates using Radio Frequency Magnetron Sputter and a large-signal piezoelectric coefficient as large as 1100 pm/V was received in lead-free $NaNbO_3$ (NNO) films, which is two times of the previous record achieved in lead-based materials.[37] This study has renewed an ongoing wide interest in lead-free piezoelectrics, which promises extensive applications in replacing toxic lead-based materials. The ultrahigh piezoelectric performance is achieved by a brand-new strategy, alkali-deficiency driven nanopillars with charged out-of-phase boundaries for a giant electromechanical response.[36] The 3D nanopillars enclosed by charged and strained 2D out-of-phase (OOP) boundaries induced by severe alkali deficiencies could act as the SFU and make a significant contribution to the piezoelectric dynamic response.[36,37]

Volatilization of alkali metals during the preparation of alkali niobate films is unavoidable, which is generally considered to be detrimental to the performance of the films, thus most previous work has focused on how to supplement alkali metals. The strategy adopted by Wu et al. can be called "turning waste into treasure." According to the first-principles calculation, in the case of Na deficiency, the formation energy of $Nb_{na/k}$ antisite defects is much smaller than that of Na vacancy, so Nb atoms tend to occupy Na vacancy to form $Nb_{na/k}$ antisite defects (Figure 8A). Nanopillars are vertically distributed in the film perpendicular to the substrate and run through the film. The fully coherent and perpendicular between the nanocolumns and the substrate indicates that the film realizes the ideal epitaxial growth (Figure 8D), which is beneficial to the performance of the film. In planar STEM images, nanopillars with sizes ranging from several to dozens of nanometers can be observed embedded in the matrix (Figure 8E), the inset shows the results of geometric phase analysis, showing that a pair of positive/negative stresses appear at the interface between the matrix and the nanopillars. The stress leads to a strong distortion between the nanocolumns and the matrix. There are relatively more Na vacancies in the smaller nanopillars, thus enriching more Nb atoms, resulting in larger lattice distortion compared with the larger nanopillars. To maintain electrical neutrality, Nb presents different valence states in regions with different enrichment degrees. As mentioned above, relatively more Nb is enriched at the out-of-phase boundaries of small-sized nanopillars, so the valence state of Nb here is lower than that at the interface of large-sized nanopillars. The decreased Nb valence at the

interface indicates that charge redistribution occurs to reduce the energy, which greatly affects the local polarization at the out-of-phase boundaries. Figure 8F shows a regular nanopillar containing 12 Nb atoms and the polarization analysis of the region. It can be found that the polarization and stress on the out-of-phase boundaries have a good corresponding relationship, that is, the positive stress region corresponds to the tail-to-tail polarization state and the negative stress region corresponds to the head-to-head polarization state. The polarization mode of head-to-head and tail-to-tail is mainly due to the fact that the bound charge on the out-of-phase boundaries breaks the continuity of polarization. This unique polarization mode makes the charged interface between the matrix and the nanocolumn in a metastable state, and at the same time makes the domain boundaries closed to form an inhomogeneous and gradually rotated strong depolarization field. The local strong depolarization field promotes polarization rotation on the charged boundaries. This polarization steering driven by the depolarization field can reach an unstable point. At this unstable point, the electric field with a small value along the c-axis direction is sufficient to lead to a large polarization rotation along the out-of-plane direction, which is manifested as the improvement of the piezoelectric dynamic response.

Wu et al. proved that lattice distortion and bound charge indeed contributed to the piezoelectric response by comparing the electric field dependence of the electric-field induced strain under four conditions: single-domain NNO film for only strained, only charged, and strained + charged NNO films (Figure 8G). Figure 8H shows the effective electric-field induced strain as a function of the frequency of the four cases in Figure 8G. The results further confirm that the huge piezoelectric response originates from the strained and the charged out-of-phase boundaries. The piezoelectric coefficient and temperature stability of several main lead-free piezoelectric ceramics, PZT ceramics, and NNO films in this study are compared (Figure 8I). Since no complex chemical doping is introduced, the films prepared by introducing the strategy of local symmetry breaking and polarization heterogeneity through the nanopillar structure have great advantages in piezoelectric coefficient and T_c.

It is seen that charged and strained domain boundaries are randomly distributed in the plane, thus the contribution of these disordered SFUs to performance has certain limitations. To further improve the influence of antiphase domain and charged domain boundaries on dynamic piezoelectric properties, one would consider regulating the ordering of such SFUs. Since it is the vertically distributed boundaries along the out-plane direction that form a closed interface that contributes to the piezoelectric dynamic response. It can be assumed that the density, morphology, size, and vertical distribution of the antiphase domain boundaries in the plane of thin films can be precisely controlled to achieve a further breakthrough in the performance of KNN-based piezoelectric thin films.

In addition to regulating the dielectric and piezoelectric properties, as a kind of SFU, some topological ferroelectric domains can be promising candidates for non-volatile memory devices. For instance, Z. W. Li et al. revealed center-type topological domains in individual nanodots, which are stable over a sufficiently long time and can be manipulated and reversibly switched by an electric field.[45] In contrast to 1D topological domains in ferroelectrics, such as the mentioned polar skyrmions which are still at the theoretical stage, the ferroelectric center-type topological SFU can already be well compatible with the existing semiconductor and integrated circuit industry by etching the electrode covered on ferroelectric films. Using this method, a prototype of non-volatile memories with high stability and fatigue resistance is obtained.[46]

In addition to piezoelectric thin films with nanopillar structures, piezoelectric ceramics with nanoscale polar regions are also examples of SFU ordering. The recently constructed various polar nanoregions could act as SFU orderings for enhanced piezoelectricity. Local structure heterogeneity, which is short-range R polar nano regions within the long-range T matrix, was pointed out in PMN–PT[47] and then expanded in lead-free (K,Na)NbO_3 (KNN).[48] The other example is the slush polar state, short-range polar nano regions with multiphase coexistence, which was proposed in PMN-PT relaxor[49] and achieved in $BaTiO_3$ and KNN-based lead-free piezoelectrics.[40,41] These SFU configurations with local symmetry breaking greatly improve the dynamic electromechanical response of piezoelectric materials.

2.5 | Thermoelectrics: Local ferromagnetic ordering as SFUs for concurrently facilitating phonon scattering and carrier transport

As the fifth case discussed in this review, thermoelectric materials have two eternal pursuits: high electrical transport and low thermal transport simultaneously, thus high overall thermoelectric performance, the figure of merit (ZT). The factors that affect ZT value are complex since they are strongly coupled with each other and present dynamic and contradictory characteristics, for example, electrical conductivity σ versus Seebeck

coefficient α, electrical conductivity σ versus thermal conductivity κ, carrier concentration n versus carrier mobility μ.[16,50] Therefore, how to decouple them and optimize electrical and thermal transport concurrently is a challenge. Reviewing the previous strategies employed in different thermoelectric systems, many of them could be seen as SFUs engineering, which is a possible key to decoding the confusion aforementioned thus optimizing thermoelectric performance. The representative examples include superparamagnetic nanoparticles,[51] clusters of interstitials,[52] ordered vacancies,[53] heterostructures between two phases,[54] nanoscale ferroelectric phases,[55] 3D modulation doping,[56] 2D layered structure,[57] 1D chain-like soft structure,[58] short-range low-symmetry nanophases,[57,59] dislocation/strain network,[52,60] and so forth, all of which always present lower symmetry and distribute in the long-range thermoelectric matrix. These SFUs not only ensure the long-range of electrical conduction but also realizes the short-range of phonon conduction.

Here, we take the superparamagnetic nanoparticles as the SFU for example to optimize thermoelectric performance. The introduction of magnetic nanoparticles could produce charge transfer and energy filtering effects which are beneficial to electrical transport, together with enhanced phonon scattering as a result of both the magnetic fluctuations and the nanostructures themselves.[51] According to Maxwell's electromagnetic theory, charged particles (electrons and holes) will move along the circular path or helix and charged carriers will be trapped by magnetic impurities in materials due to Lorentz force. In previous reports, it is necessary to eliminate magnetic impurities to realize outstanding electrical properties for all semiconductor materials. A new idea is to embed magnetic nanoparticles as local SFU into the long-range thermoelectric matrix to form local symmetry breaking, which is expected to manipulate electron and phonon transport simultaneously. The magnetic moments of atoms in magnetic nanoparticles point in the same direction to form an orderly arranged single-domain, which can be used to enhance the properties of thermoelectric materials. The presence of magnetic nanoparticles induces the enhancement of interface scattering which can reduce the thermal conductivity. Additionally, the internal magnetic moment not only produces the magnetoelectric effect of electron spiral motion and magnon-drag thermopower but also trap electrons, so as to realize the regulation of carriers.

Zhao et al. reported the idea of changing permanent magnetic nanoparticles from ferromagnetism to paramagnetism,[61] which was employed to reduce the performance attenuation of thermoelectric materials in the inherent excitation region. A series of magnetic nanocomposite thermoelectric materials are prepared by adding M-type barium ferrite ($BaFe_{12}O_9$) nanoparticles (BaM-NPs) into matrix $CoSb_3$. BaM-NPs are in a ferromagnetic state when working temperature (T_W) is lower than T_c, producing a nonuniform spherical magnetic field and trapping electrons due to spiral motion. When $T_W > T_c$, BaM-NPs are in the paramagnetic state and the spherical magnetic will disappear, releasing the trapped electrons, which increases the carrier concentration and the Seebeck coefficient. BaM-NPs act as an "electron memory." Zhao et al. reported that by embedding nanoparticles of a soft magnetic material (Co nanoparticles) in a thermoelectric matrix ($CoSb_3$), shown in Figure 7E–G achieves dual control of phonon- and electron-transport properties.[51] The superparamagnetic behavior of nanoparticles leads to three kinds of thermo-electromagnetic effects, as shown in Figure 7B–D: charge transfer from magnetic inclusion to matrix; multiple electron scattering as a result of superparamagnetic fluctuations; enhanced phonon scattering caused by magnetic fluctuations and nanostructures. The existence of magnetic nanoparticles improves σ and α, reduces the thermal conductivity, and greatly improves ZT, with a maximum value of 1.8, as shown in Figure 7H–K.

In the case above, both the randomly oriented spins within the magnetic domains and the nanostructure interfaces enhance phonon scattering. However, the disorder of magnetic moments, to some extent, may deteriorate the carrier transport properties simultaneously. One can envisage a hierarchical structure consisting of nanoscale magnetic-particle SFUs, that is, small particles are concentrated together to form a medium-sized agglomeration area, and there are relatively fewer nanoparticles between the agglomeration areas. The hierarchical ordering structure at the micro/nano scales can cooperate with the magnetic fluctuations at the atomic scale to realize the multiple scattering of phonons with different wavelengths. At the same time, the regions between SFUs can be used as the carrier transport channels, which makes the carrier transport tend to be orderly. Therefore, it is expected to achieve the simultaneous optimization of electro-phonon transports.

2.6 | Conducting nanofilaments as SFUs in $SrFeO_x$ epitaxial thin films with topotactic phase transformation for high-density resistive switching memory

The sixth case is topotactic phase-change materials based on SFU ordering, which is an ideal candidate for

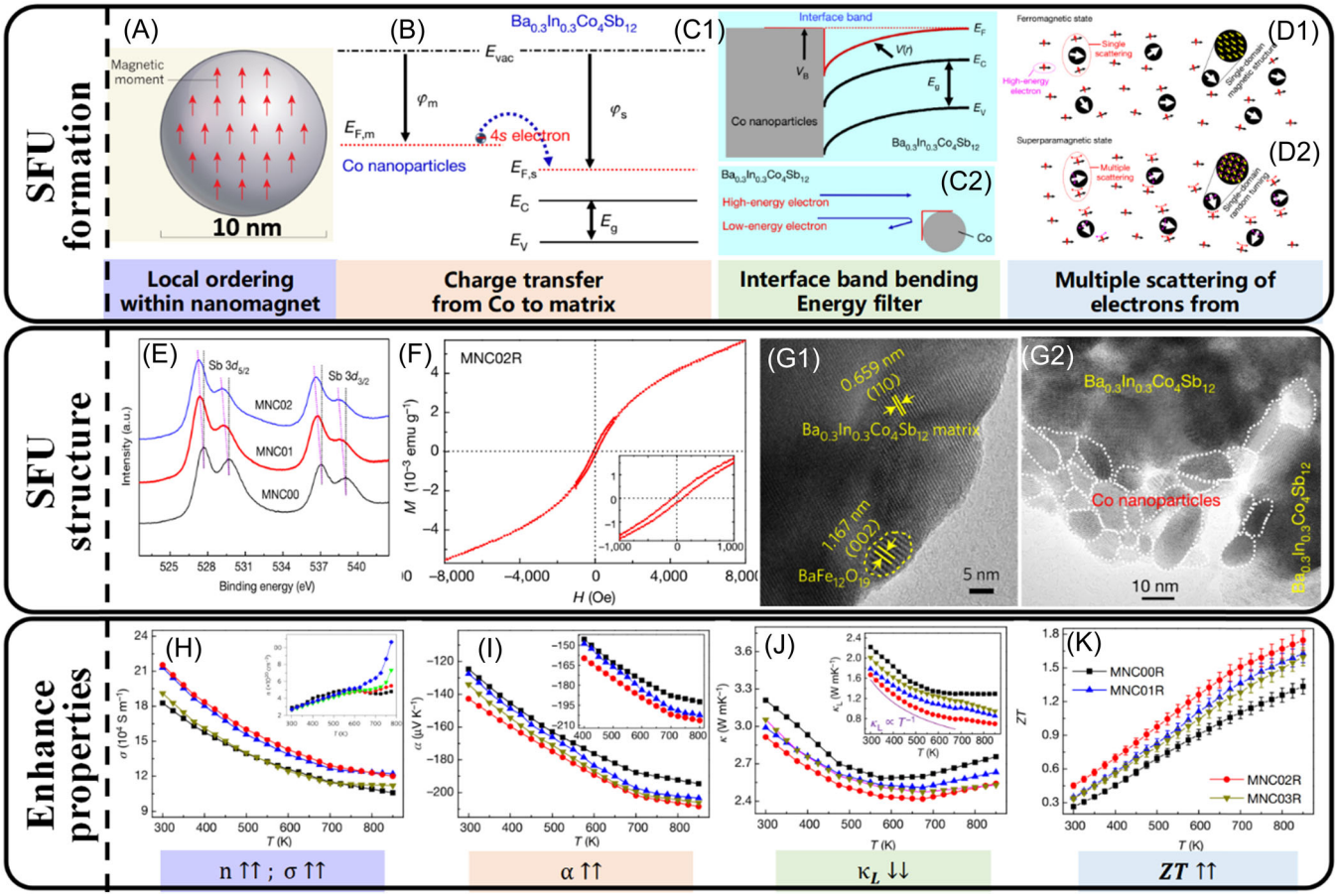

FIGURE 7 Enhanced thermoelectricity through a local ferromagnetic structure (SFU) in magnetic nanocomposite (MNC) thermoelectric materials. (A) Schematic for local magnetic-moment ordering within nanomagnet. (B) Schematic of the charge transfer of 4 s electrons from the Co nanoparticles to the MNC matrix. (C1) Interface band bending away from the interface induced by the charge transfer of Co 4 s electrons from the Co nanoparticles to the MNC matrix. (C2) Electron scattering as a result of band bending at the interface between Co nanoparticles and MNC matrix. (D1, D2) Schematics for the single scattering of electrons due to ferromagnetic Co nanoparticles and multiple scattering of electrons due to superparamagnetic Co nanoparticles. (E) XPS of Sb 3d core levels of $xCo/Ba_{0.3}In_{0.3}Co_4Sb_{12}$ composites. (F) Magnetization versus magnetic field (M–H) plot for the composite, showing the existence of the magnetic feature. (G1, G2) TEM images of two composites, showing the magnetic nanoparticles. (H–K) Temperature dependence of electrical and thermal properties of $xCo/Ba_{0.3}In_{0.3}Co_4Sb_{12}$ composites: (H) the electric conductivity σ with carrier concentration n inset, (I) Seebeck coefficient α, (J) thermal conductivity κ with lattice thermal conductivity κ_{latt} inset, and figure of merit ZT. (A) Reproduced with permission from Boona,[62] copyright 2017 Springer Nature. (B–F, G2, H–K) Reproduced with permission from Zhao et al.,[51] copyright 2018 Springer Nature. (G1) Reproduced with permission from Zhao et al.,[61] copyright 2017 Springer Nature. SFU, structural-functional unit; TEM, transmission electron microscope; XPS, X-ray photoelectron spectroscopy.

brain-like computing. To break through the bottleneck of power and computing speed based on the existing von Neumann architecture, the development of brain-like computing chips is a promising method, and the core of this technology is to find a new storage material and device with similar human brain synapse function. Compared with the magnetic storage (MMRAM) and ferroelectric storage (FRAM) mentioned above, resistive storage (RRAM) has lower energy consumption, faster speed, and simpler structure, which is more suitable for artificial synapses and neural networks for computing.

The transition metal oxides (TMOs) typically possess a widely tunable oxygen stoichiometry, which leads to a variety of crystalline phases and rich functional properties. For example, with respect to an electric field, the $SrFeO_x$ (SFO) (and its analog, $SrCoO_x$)[63] can exhibit a reversible topotactic phase transformation between the insulating brownmillerite $SrFeO_{2.5}$ (BM-SFO) and the conducting perovskite $SrFeO_3$ (PV-SFO) phases (Figure 8A1,A2). Such electric-field-induced conversion of conductivity and insulation, along with dramatic changes in the transport, magnetic, and optical properties[16,64] are the basis for its application in resistive switching (RS) memories. Developing all-solid-state

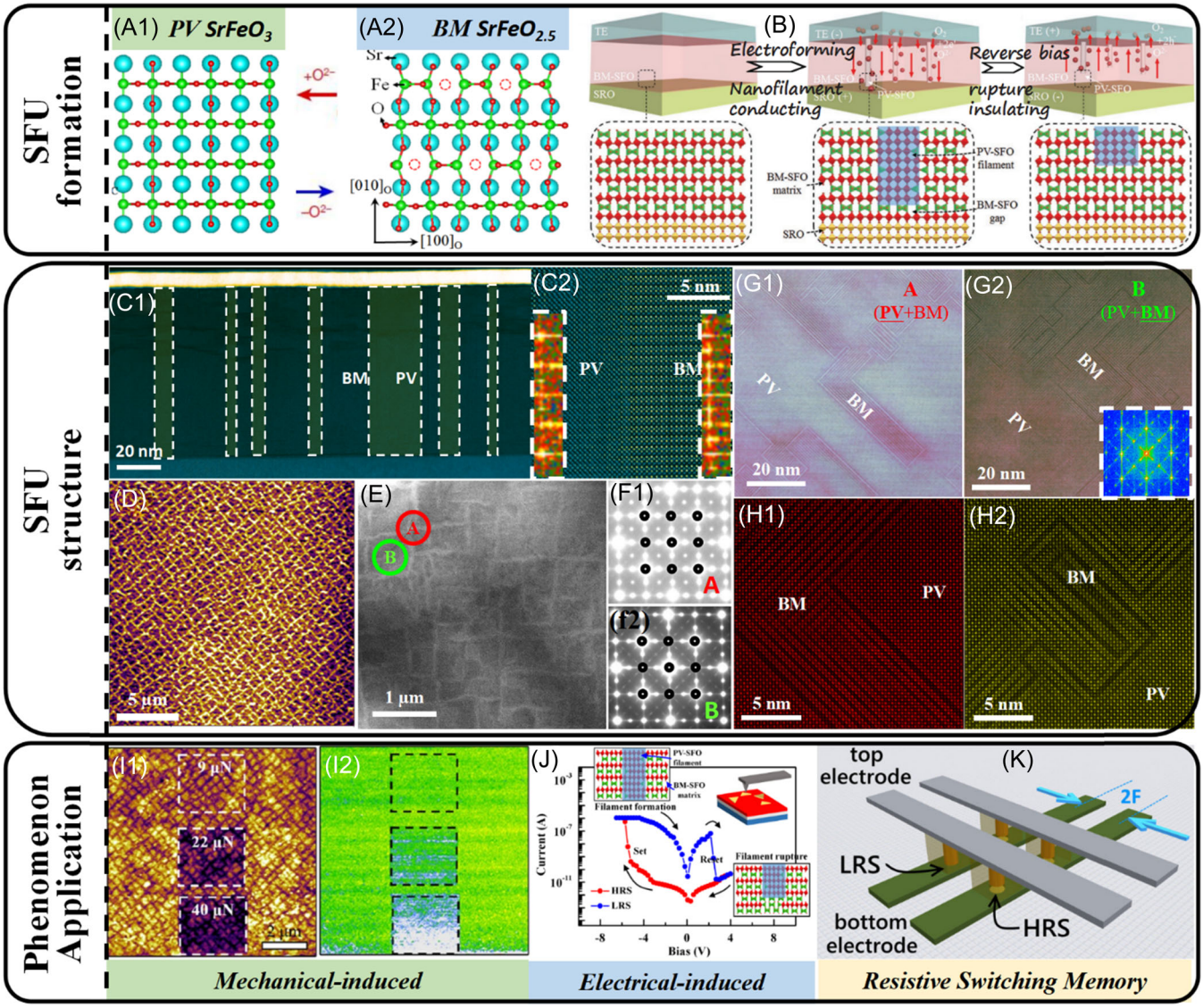

FIGURE 8 Conducting nanofilaments in topotactic phase transformation. (A1, A2) SFU formation: Crystal structures and topotactic phase transformation of $SrFeO_3$ and $SrFeO_{2.5}$ due to oxygen vacancy ordering. (B) Schematics showing mechanisms of nanofilament formation and resistive switching. (C–H) Hierarchical structures of phase-coexisted nanofilaments. (C1, C2) STEM HAADF cross-section image showing nanofilaments vertically grown within the film. (D) AFM topography image of the mixed-phase SFO film. (E) TEM ABF plan-view image. (F1, F2) Electron diffraction patterns from the two regions marked as *A* and *B* in (d), respectively. (G1, G2) High-resolution STEM ABF images showing *A* region as BM within PV matrix and *B* region as PV within BM matrix. (H1, H2) Enlarged images showing the phase coexistence from (G1, G2). (I1, I2) Mechanical stress-induced phase transformation: AFM topography image (I1) and C-AFM current map (I2). (J) Resistive switching properties of Au/SFO/$SrRuO_3$ (SRO) nanocapacitor devices. (K) Schematic showing high-density resistive switching memory.[42,43] (A–C, J) Reproduced with permission from Tian et al.,[42] copyright 2019 John Wiley and Sons. (D–I) Reproduced with permission from Tian et al.,[43] copyright 2020 American Chemical Society. (K) Reproduced with permission from Lim and Ismail,[44] copyright 2015 MDPI. ABF, annular bright field; HAADF, high-angle annular dark field; SFU, structural-functional unit; STEM, scanning transmission electron microscope; TEM, transmission electron microscope; XPS, X-ray photoelectron spectroscopy.

SFO-based RS memories is in great demand. Tian et al. embedded nanoscale PV-SFU nanofilaments into BM-SFU matrix to obtain a nanoscaffold-like two-phase hybrid configuration, this new phase coexistence form contributes to multi-field-induced topotactic phase transition, showing excellent storage performance.[42] The SFUs in this case are the nanofilaments, which are used as the resistance switch in the topotactic phase film and the research on the size, density, distribution as well as filamentation mechanism of nanofilaments is of great significance to guide the ultimate scalability of RS memories based on SFUs.

Some recent studies demonstrated the RS phenomenon in SFO-based capacitor-like heterostructures and proposed a filamentary mechanism for RS,[16e] that is, an

electric field-induced local topotactic phase transformation between BM-SFO and PV-SFO, Figure 8B. Here the conducting nanofilament is a representative example of SFUs in topotactic-phase films for resistive switching. The direct observation of conductive filaments consisting of PV-SFO is important to making the filamentary mechanism convincing and guide the ultimate scalability of SFO-based RS memories since the size of conductive filaments is critical. In addition, the downscaling of SFO-based RS cells to the nanometer range is a huge challenge in experiment, leaving it a mystery as to whether the TMOs-based RS memories are potentially useful for high-density memory applications. Tian et al. conducted a comprehensive study on phase transformation and RS behavior in SFO epitaxial thin films.[42,43] It revealed that PV-SFO nanofilaments (average diameter: ~10 nm) embedded within the BM-SFO matrix in the ON-state device, Figure 8C1,C2, providing direct evidence for the filamentary mechanism of RS. The reversible changes in both surface height and conductance in the SFO films upon applying electric fields demonstrate that the local phase transformation between BM-SFO and PV-SFO can be reversibly controlled by the electric field. Tian et al. further achieved SFO epitaxial thin films with a nanoscale mixture of BM-SFO and PV-SFO phases by finely controlling the oxygen pressure during the film growth. The mixed-phase SFO film in its pristine state exhibits a nanoscaffold structure consisting of PV-SFO nanodomains embedded into the BM-SFO matrix, Figure 8D–H. This novel phase coexistence gives rise to multifield-induced topotactic phase transformation. Nanoscale phase evolution and associated responses of current and electrochemical strain could be achieved upon applications of both electrical and mechanical stimuli. Particularly, an ON/OFF conductance ratio of ~10 and an electrochemical strain as large as ~1.3% are obtained, Figure 8I,J. Based on these materials, Au/SFO/$SrRuO_3$ (SRO) nanocapacitor devices were developed, which are downscaled to a lateral size of ~180 nm. These devices present excellent memory performance including large ON/OFF ratio of ~10^4, long retention time of >10^5 s, and high endurance of >10^7 cycles, which already compares favorably with commercial flash memory, Figure 8J–K. These studies therefore not only advance the fundamental understanding of the RS mechanism in TMOs exhibiting multifield control of topotactic phase transformation but also underscore the great potential of these materials for use in high-density RS memories.[42,43]

From the perspective of applications, the perpendicular generation of the nanofilament SFUs between the top and bottom electrodes contributes to a favorably narrow distribution of switching parameters in RRAM. It would be more promising if we could artificially regulate the ordering of the nanofilament SFUs to make them uniformly distributed in the plane and grow toward the direction we want.

3 | CONCLUSION AND PERSPECTIVES

Employing SFU ordering to study electron-correlated materials can help us understand the origin of various novel properties more intuitively. The diversity of SFU types and scales corresponds to the various construction methods, implying its infinite possibility. Designing SFU based on specific functions rather than chemical elements can get rid of the limitation of elements, and its advantages have been preliminarily reflected in the electron-correlated materials introduced above.

This review attempts to study several typical functional materials from the perspective of SFUs and their orderings. One can understand the macroscopic performance of the materials through the properties of SFUs. For example, the overlap and contact between SFUs composed of hydrogen-like orbitals and Fe ions in ferromagnetic semiconductors trigger the generation of magnetic moments; the metastable state of the electric dipole on the 2D OOP boundaries in the piezoelectric film has made a great contribution to its piezoelectric dynamic response. The intrinsic magnetic fluctuation of magnetic nanoparticles in the thermoelectric matrix and their electron exchange with the matrix simultaneously regulate electron and phonon transport. In addition, SFU functionality is directly linked to its possible application, for example, the nanoscale topological structure of the polar/spin skyrmions and the theoretically ultra-small driving current make it a candidate for a new generation of a nonvolatile storage device; the electrical conductivity and controllable characteristics of nanofilaments are the basis for RS memory. The regulation of SFU ordering further enlarges the effect of SFUs on macroscopic properties to some extent, for example, the antiphase domain boundaries in piezoelectric films can be further regulated along the in-plane uniformly and perpendicular to the substrate. In some cases, the ordering of SFUs is closely related to the synergistic effect between SFUs, for example, our proposed hierarchical structure composed of densely and sparsely distributed magnetic nanoparticles and the artificial lattice realized by creating a linear array of skyrmions. We have to say, the SFU ordering strategy is still in its infancy, which means it has broad prospects, but a long way to go.

With the development of material characterization and synthesis technology, the SFUs, and the ordering hold much potential for further optimization and are

well controlled. Taking SFU ordering illustrated in this review, some future directions are proposed as follows:

(1) Ferromagnetic metals. The current microscopic characterization techniques can only show the 2D projection of the skyrmions to a large degree, but the actual skyrmion is not seemed like a "particle," but a "tube," which is 3D. As the carrier of information, the "tube" is obviously not conducive to high-speed, free movement and regulation, which hinders its practical application. To solve this problem, a new technique is needed to "layer-by-layer cut" the skyrmions to restore their 3D structure.
(2) Ferroelectric thin films. The stable topological structures induced by the interface strain of the thin films have been introduced, but it is unpractical for real applications and it is difficult to introduce such strain in bulk materials. As a compromise solution, nanodots can be introduced, and the high energy state of the surface also causes a strong depolarization field, so as to obtain polar topological structures.
(3) Piezoelectric material. The coupling between SFUs, such as density or distribution, has a great influence on the material properties. In this review, it is clear that the OOP boundaries as SFUs have a great contribution to the piezoelectric dynamic response. Therefore, it is interesting how to improve the density of columnar domains in thin films, and further, how to distribute them orderly in the plane direction.
(4) Topotactic phase-change materials. The on (conductive) and off (insulated) switching states of conductive filaments are the basis of topotactic phase-change materials used in RS memory, so the density of conductive filaments directly determines the size and storage density of the device. In future work, how to minimize the diameter and regulate the ordering of the conductive filaments, meanwhile ensuring their stability and reversibility, are urgent to probe.

We need more advanced and comprehensive technologies to study and construct SFU ordering in various material systems. In fact, SFU orderings mentioned in this review are only the tip of the iceberg of the functional material family, and SFUs of different types and scales are widespread. For instance, Schottky heterojunction ordering can be introduced into the thermoelectric systems to reduce the timeliness of thermoelectric performance due to its hindering effect on ion migration,[54] moreover, the introduction of short-range ferroelectric polar nanoregions to provide local strong non-resonance, thereby synergistically affecting carrier and phonon transport.[55] To clarify the rules of various types of SFU orderings, or rather, the interaction between their structural features and corresponding functions, in the following work, we should use in-situ electron microscopy techniques to study the responses of different SFUs under external stimuli. In addition, the in-situ characterization technologies can be used to realize the construction and regulation of their ordering, for example, polar skyrmions.

In future work, SFUs can be further classified. Taking SFUs in the above electron-correlated materials, for example, one may divide them into 1D (e.g., magnetic nanoparticles), 2D (e.g., charged interface), and 3D (e.g., spin/polar topologies) by dimension. The dimension of ordering can show its properties to a certain extent. For example, 1D ordering is often constructed in a simple way, but the difficulty is the distribution in the matrix (e.g., how to ensure non-agglomeration); 2D ordering is usually associated with the interface effect, so it is often constructed in thin film materials. To construct 2D ordering in bulk materials, it is often necessary to introduce stress or some special structures. The stability and controllability of 3D ordering (e.g., skyrmions) are often the key to their practical application. A more important benefit of classifying SFUs is that different criteria are needed for understanding and designing different types of SFUs. For SFUs at the 1D or 2D scale, the quantum confinement effect sometimes would be the dominant function; for SFUs at the larger 3D scale, no short-range force such as the strong force in the nucleus is needed to be considered, and so forth.

The strategy of SFU ordering has high universality and flexibility. The research idea of SFU ordering is expected to be extended to, in addition to the electron-correlated material systems, the development of the next generation of information technology core materials, ultrahigh performance structural materials, future-oriented energy conversion and storage materials, high-performance biomedical materials, and other materials systems. In addition, combining the strategy of SFU ordering with computational materials science, the development of reverse design, optimization design method, software, and database of materials will greatly accelerate the development of new materials.

There are relatively few studies on SFU ordering. A case in point is that no corresponding work, up to now, has been published on the regulation of nanoparticles in thermoelectric nor 2D OOP boundaries in piezoelectric films. On the one hand, it is hindered by the development of material synthesis and characterization technologies, and on the other hand, our understanding of SFUs is still not deep enough.

ACKNOWLEDGMENTS

The authors would like to acknowledge the financial support from the National Key R&D Program of China (2021YFB3201100), the National Natural Science Foundation of China (52172128), and the Top Young Talents Programme of Xi'an Jiaotong University. The authors would like to thank the strong support from the Instrumental Analysis Center of Xi'an Jiaotong University.

CONFLICT OF INTEREST

The authors declare no conflict of interest.

ORCID

Haijun Wu http://orcid.org/0000-0002-7303-379X

REFERENCES

[1] Anderson PW. More is different. *Science*. 1972;177(4047):393-396. doi:10.1126/science.177.4047.393

[2] Turkel S, Swann J, Zhu Z, et al. Orderly disorder in magic-angle twisted trilayer graphene. *Science*. 2022;376(6589):193-199. doi:10.1126/science.abk1895

[3] Guo HW, Hu Z, Liu ZB, Tian JG. Stacking of 2D materials. *Adv Funct Mater*. 2021;31(4):2007810. doi:10.1002/adfm.202007810

[4] a) Kivshar Y. All-dielectric meta-optics and non-linear nanophotonics. *Natl Sci Rev*. 2018;5(2):144-158. doi:10.1093/nsr/nwy017; b) Zhao H, Feng L. Parity–time symmetric photonics. *Natl Sci Rev*. 2018;5(2):183-199. doi:10.1093/nsr/nwy011; c) Luo X. Plasmonic metalens for nanofabrication. *Natl Sci Rev*. 2017;5(2):137-138. doi:10.1093/nsr/nwx135

[5] Ge H, Yang M, Ma C, et al. Breaking the barriers: advances in acoustic functional materials. *Natl Sci Rev*. 2017;5(2):159-182. doi:10.1093/nsr/nwx154

[6] Sklan SR, Li B. Thermal metamaterials: functions and prospects. *Natl Sci Rev*. 2018;5(2):138-141. doi:10.1093/nsr/nwy005

[7] Ball P. Bending the laws of optics with metamaterials: an interview with John Pendry. *Natl Sci Rev*. 2017;5(2):200-202. doi:10.1093/nsr/nwx118

[8] a) Liu XC, Zhang HW, Lu K. Strain-induced ultrahard and ultrastable nanolaminated structure in nickel. *Science*. 2013;342(6156):337-340. doi:10.1126/science.1242578; b) Zong H, Wu H, Tao X, et al. Percolated strain networks and universal scaling properties of strain glasses. *Phys Rev Lett*. 2019;123(1):015701. doi:10.1103/PhysRevLett.123.015701; c) Xu W, Zhang B, Li XY, Lu K. Suppressing atomic diffusion with the Schwarz crystal structure in supersaturated Al–Mg alloys. *Science*. 2021;373(6555):683-687. doi:10.1126/science.abh0700

[9] Luo W, Yan S, Zhou J. Ceramic-based dielectric metamaterials. *Interdiscip Mater*. 2022;1:11-27. doi:10.1002/idm2.12012

[10] Chen W, Gu J, Liu Q, et al. Two-dimensional quantum-sheet films with sub-1.2 nm channels for ultrahigh-rate electrochemical capacitance. *Nat Nanotechnol*. 2021;17:153-158. doi:10.1038/s41565-021-01020-0

[11] a) Li X, Wu H, Elshahawy AM, et al. Cactus-Like NiCoP/NiCo-OH 3D architecture with tunable composition for high-performance electrochemical capacitors. *Adv Funct Mater*. 2018;28(20):1800036. doi:10.1002/adfm.201800036; b) Guan C, Sumboja A, Wu H, et al. Hollow Co_3O_4 nanosphere embedded in carbon arrays for stable and flexible Solid-State Zinc-Air batteries. *Adv Mater*. 2017;29(44):1704117. doi:10.1002/adma.201704117; c) Guan C, Xiao W, Wu H, et al. Hollow Mo-doped CoP nanoarrays for efficient overall water splitting. *Nano Energy*. 2018;48:73-80. doi:10.1016/j.nanoen.2018.03.034; d) Guan C, Liu X, Elshahawy AM, et al. Metal–organic framework derived hollow CoS_2 nanotube arrays: an efficient bifunctional electrocatalyst for overall water splitting. *Nanoscale Horiz*. 2017;2(6):342-348. doi:10.1039/C7NH00079K

[12] Zhang L, Zhu J, Li X, et al. Nurturing the marriages of single atoms with atomic clusters and nanoparticles for better heterogeneous electrocatalysis. *Interdiscip Mater*. 2022;1:51-87. doi:10.1002/idm2.12011

[13] Xiong F, Jiang Y, Cheng L, et al. Low-strain TiP_2O_7 with three-dimensional ion channels as long-life and high-rate anode material for Mg-ion batteries. *Interdiscip Mater*. 2022;1:140-147. doi:10.1002/idm2.12004

[14] a) Eerenstein W, Mathur ND, Scott JF. Multiferroic and magnetoelectric materials. *Nature*. 2006;442(7104):759-765. doi:10.1038/nature05023; b) Spaldin NA, Ramesh R. Advances in magnetoelectric multiferroics. *Nat Mater*. 2019;18(3):203-212. doi:10.1038/s41563-018-0275-2; c) Yang Y, Luo Z, Wu H, et al. Anomalous hall magnetoresistance in a ferromagnet. *Nat Commun*. 2018;9(1):2255. doi:10.1038/s41467-018-04712-9

[15] a) Chen S, Yuan S, Hou Z, et al. Recent progress on topological structures in ferroic thin films and heterostructures. *Adv Mater*. 2021;33(6):2000857. doi:10.1002/adma.202000857; b) Meier D, Selbach SM. Ferroelectric domain walls for nanotechnology. *Nat Rev Mater*. 2021;7:157-173. doi:10.1038/s41578-021-00375-z; c) Martin LW, Rappe AM. Thin-film ferroelectric materials and their applications. *Nat Rev Mater*. 2016;2(2):16087. doi:10.1038/natrevmats.2016.87

[16] a) Yan Q, Kanatzidis MG. High-performance thermoelectrics and challenges for practical devices. *Nat Mater*. 2021;21:503-513. doi:10.1038/s41563-021-01109-w; b) Mao J, Chen G, Ren Z. Thermoelectric cooling materials. *Nat Mater*. 2021;20(4):454-461. doi:10.1038/s41563-020-00852-w; c) Snyder GJ, Toberer ES. Complex thermoelectric materials. *Nat Mater*. 2008;7:105-114. doi:10.1038/nmat2090; d) Zhu T, Liu Y, Fu C, Heremans JP, Snyder JG, Zhao X. Compromise and synergy in high-efficiency thermoelectric materials. *Adv Mater*. 2017;29(14):1605884. doi:10.1002/adma.201605884; e) Waser R, Aono M. Nanoionics-based resistive switching memories. *Nat Mater*. 2007;6(11):833-840. doi:10.1038/nmat2023; f) Nallagatla VR, Heisig T, Baeumer C, et al. Topotactic phase transition driving memristive behavior. *Adv Mater*. 2019;31(40):1903391. doi:10.1002/adma.201903391

[17] Wang Z, Wu H, Burr GW, et al. Resistive switching materials for information processing. *Nat Rev Mater*. 2020;5(3):173-195. doi:10.1038/s41578-019-0159-3

[18] a) Story T, Gałązka RR, Frankel RB, Wolff PA. Carrier-concentration–induced ferromagnetism in PbSnMnTe. *Phys Rev Lett*. 1986;56(7):777-779. doi:10.1103/PhysRevLett.56.777;

b) Ohno H, Chiba D, Matsukura F, et al. Electric-field control of ferromagnetism. *Nature*. 2000;408(6815):944-946. doi:10.1038/35050040

[19] a) Hu L, Chen J, Fan L, et al. High-Curie-temperature ferromagnetism in (Sc,Fe)F_3 fluorides and its dependence on chemical valence. *Adv Mater*. 2015;27(31):4592-4596. doi:10.1002/adma.201500868; b) Hu L, Chen J, Fan L, et al. Zero thermal expansion and ferromagnetism in cubic $Sc_{1-x}M_xF_3$ (M = Ga, Fe) over a wide temperature range. *J Am Chem Soc*. 2014;136(39):13566-13569. doi:10.1021/ja5077487

[20] Meier D, Selbach SM. Ferroelectric domain walls for nanotechnology. *Nat Rev Mater*. 2022;7(3):157-173. doi:10.1038/s41578-021-00375-z

[21] Wachowiak A, Wiebe J, Bode M, Pietzsch O, Morgenstern M, Wiesendanger R. Direct observation of internal spin structure of magnetic vortex cores. *Science*. 2002;298(5593):577-80. doi:10.1126/science.1075302

[22] a) Du H, Che R, Kong L, et al. Edge-mediated skyrmion chain and its collective dynamics in a confined geometry. *Nat Commun*. 2015;6(1):8504. doi:10.1038/ncomms9504; b) Kézsmárki I, Bordács S, Milde P, et al. Néel-type skyrmion lattice with confined orientation in the polar magnetic semiconductor GaV_4S_8. *Nat Mater*. 2015;14(11):1116-1122. doi:10.1038/nmat4402; c) Yu XZ, Onose Y, Kanazawa N, et al. Real-space observation of a two-dimensional skyrmion crystal. *Nature*. 2010;465(7300):901-904. doi:10.1038/nature09124; d) Mühlbauer S, Binz B, Jonietz F, et al. Skyrmion lattice in a chiral magnet. *Science*. 2009;323(5916):915-919. doi:10.1126/science.1166767

[23] Yu XZ, Koshibae W, Tokunaga Y, et al. Transformation between meron and skyrmion topological spin textures in a chiral magnet. *Nature*. 2018;564(7734):95-98. doi:10.1038/s41586-018-0745-3

[24] Rößler UK, Bogdanov AN, Pfleiderer C. Spontaneous skyrmion ground states in magnetic metals. *Nature*. 2006;442(7104):797-801. doi:10.1038/nature05056

[25] a) Jia C-L, Urban KW, Alexe M, Hesse D, Vrejoiu I. Direct observation of continuous electric dipole rotation in flux-closure domains in ferroelectric $Pb(Zr,Ti)O_3$. *Science*. 2011;331(6023):1420-1423. doi:10.1126/science.1200605; b) Tang YL, Zhu YL, Ma XL, et al. Observation of a periodic array of flux-closure quadrants in strained ferroelectric $PbTiO_3$ films. *Science*. 2015;348(6234):547-551. doi:10.1126/science.1259869; c) Nelson CT, Winchester B, Zhang Y, et al. Spontaneous vortex nanodomain arrays at ferroelectric heterointerfaces. *Nano Lett*. 2011;11(2):828-834. doi:10.1021/nl1041808

[26] Wang YJ, Feng YP, Zhu YL, et al. Polar meron lattice in strained oxide ferroelectrics. *Nat Mater*. 2020;19(8):881-886. doi:10.1038/s41563-020-0694-8

[27] a) Abid AY, Sun Y, Hou X, et al. Creating polar antivortex in $PbTiO_3/SrTiO_3$ superlattice. *Nat Commun*. 2021;12(1):2054. doi:10.1038/s41467-021-22356-0; b) Yadav AK, Nelson CT, Hsu SL, et al. Observation of polar vortices in oxide superlattices. *Nature*. 2016;530(7589):198-201. doi:10.1038/nature16463

[28] Das S, Tang YL, Hong Z, et al. Observation of room-temperature polar skyrmions. *Nature*. 2019;568(7752):368-372. doi:10.1038/s41586-019-1092-8

[29] Gong F-H, Tang Y-L, Zhu Y-L, et al. Atomic mapping of periodic dipole waves in ferroelectric oxide. *Sci Adv*. 2021;7(28):eabg5503. doi:10.1126/sciadv.abg5503

[30] Jiang AQ, Geng WP, Lv P, et al. Ferroelectric domain wall memory with embedded selector realized in $LiNbO_3$ single crystals integrated on Si wafers. *Nat Mater*. 2020;19(11):1188-1194. doi:10.1038/s41563-020-0702-z

[31] Fert A, Reyren N, Cros V. Magnetic skyrmions: advances in physics and potential applications. *Nat Rev Mater*. 2017;2(7):17031. doi:10.1038/natrevmats.2017.31

[32] a) Jin C, Song C, Wang J, Liu Q. Dynamics of antiferromagnetic skyrmion driven by the spin hall effect. *Appl Phys Lett*. 2016;109(18):182404. doi:10.1063/1.4967006; b) Zhang X, Zhou Y, Ezawa M. Antiferromagnetic skyrmion: stability, creation and manipulation. *Sci Rep*. 2016;6:24795. doi:10.1038/srep24795

[33] Ma F, Zhou Y, Braun HB, Lew WS. Skyrmion-based dynamic magnonic crystal. *Nano Lett*. 2015;15(6):4029-4036. doi:10.1021/acs.nanolett.5b00996

[34] Tan C, Dong Y, Sun Y, et al. Engineering polar vortex from topologically trivial domain architecture. *Nat Commun*. 2021;12(1):4620. doi:10.1038/s41467-021-24922-y

[35] Tan CB, Zhong XL, Wang JB. Polar topological structures in ferroelectric materials. *Acta Phys Sin*. 2020;69(12):127702. doi:10.7498/aps.69.20200311

[36] Wu H, Ning S, Waqar M, et al. Alkali-deficiency driven charged out-of-phase boundaries for giant electromechanical response. *Nat Commun*. 2021;12(1):2841. doi:10.1038/s41467-021-23107-x

[37] Liu H, Wu H, Ong KP, et al. Giant piezoelectricity in oxide thin films with nanopillar structure. *Science*. 2020;369(6501):292-297. doi:10.1126/science.abb3209

[38] Yin J, Zong H, Tao H, et al. Nanoscale bubble domains with polar topologies in bulk ferroelectrics. *Nat Commun*. 2021;12(1):3632. doi:10.1038/s41467-021-23863-w

[39] a) Waqar M, Wu H, Chen J, Yao K, Wang J. Evolution from Lead-Based to Lead-Free piezoelectrics: engineering of lattices, domains, boundaries, and defects leading to giant response. *Adv Mater*. 2022;34:2106845. doi:10.1002/adma.202106845; b) Wu H, Zhang Y, Wu J, Wang J, Pennycook SJ. Microstructural origins of high piezoelectric performance: a pathway to practical Lead-Free materials. *Adv Funct Mater*. 2019;29(33):1902911. doi:10.1002/adfm.201902911

[40] a) Zhang Y, Xue D, Wu H, Ding X, Lookman T, Ren X. Adaptive ferroelectric state at morphotropic phase boundary: coexisting tetragonal and rhombohedral phases. *Acta Mater*. 2014;71:176-184. doi:10.1016/j.actamat.2014.03.007; b) Muhtar Ahart1 MS, Cohen RE. *Nature*. 2008;.; c) Wu H, Xue D, Lv D, et al. Microstructure at morphotropic phase boundary in $Pb(Mg_{1/3}Nb_{2/3})O_3$-$PbTiO_3$ ceramic: coexistence of nano-scaled {110}-type rhombohedral twin and {110}-type tetragonal twin. *J Appl Phys*. 2012;112(5):052004. doi:10.1063/1.4745935; d) Gao J, Xue D, Wang Y, et al. Microstructure basis for strong piezoelectricity in pb-free Ba$(Zr_{0.2}Ti_{0.8})O_3$-$(Ba_{0.7}Ca_{0.3})TiO_3$ ceramics. *Appl Phys Lett*. 2011;99(9):092901. doi:10.1063/1.3629784; e) Zhang Y, Qu W, Peng G, et al. Seeing structural mechanisms of optimized piezoelectric and thermoelectric bulk materials through structural defect engineering. *Materials*. 2022;15(2):487. doi:10.3390/ma15020487; f) Zhang N, Zheng T, Li N, et al. Symmetry of the

underlying lattice in (K,Na)NbO_3-Based relaxor ferroelectrics with large electromechanical response. *ACS Appl Mater Interfaces*. 2021;13(6):7461-7469. doi:10.1021/acsami.0c21181

[41] a) Wu B, Wu H, Wu J, Xiao D, Zhu J, Pennycook SJ. Giant piezoelectricity and high curie temperature in nanostructured alkali niobate lead-free piezoceramics through phase coexistence. *J Am Chem Soc*. 2016;138(47):15459-15464. doi:10.1021/jacs.6b09024; b) Zheng T, Wu H, Yuan Y, et al. *Energy Environ Sci*. 2017;10(2):528. doi:10.1039/C6EE03597C; c) Zhao C, Wu H, Li F, et al. Outstanding piezoelectric performance in lead-free 0.95(K,Na)(Sb,Nb)O_3-0.05(Bi,Na,K)ZrO_3 thick films with oriented nanophase coexistence. *Adv Electron Mater*. 2019;5(4):1800691. doi:10.1002/aelm.201800691; e) Tao H, Wu H, Liu Y, et al. Ultrahigh performance in Lead-Free piezoceramics utilizing a relaxor slush polar state with multiphase coexistence. *J Am Chem Soc*. 2019;141(35):13987-13994. doi:10.1021/jacs.9b07188; f) Tao H, Yin J, Zhao C, Wu H, Wu J. New role of relaxor multiphase coexistence in potassium sodium niobate ceramics: reduced electric field dependence of strain temperature stability. *ACS Appl Mater Interfaces*. 2020;12(44):49822-49829. doi:10.1021/acsami.0c15496; g) Lee MH, Kim DJ, Park JS, et al. High-Performance Lead-Free piezoceramics with high curie temperatures. *Adv Mater*. 2015;27(43):6976-6982. doi:10.1002/adma.201502424; h) Li P, Zhai J, Shen B, et al. Ultrahigh piezoelectric properties in textured (K,Na)NbO_3-based lead-free ceramics. *Adv Mater*. 2018;30(8):1705171. doi:10.1002/adma.201705171; i) Hu C, Meng X, Zhang M-H, et al. Ultra-large electric field–induced strain in potassium sodium niobate crystals. *Sci Adv*. 2020;6(13):eaay5979. doi:10.1126/sciadv.aay5979; j) Liu Q, Zhang Y, Gao J, et al. Practical high-performance lead-free piezoelectrics: structural flexibility beyond utilizing multiphase coexistence. *Natl Sci Rev*. 2019;7(2):355-365. doi:10.1093/nsr/nwz167

[42] Tian J, Wu H, Fan Z, et al. Nanoscale topotactic phase transformation in $SrFeO_x$ epitaxial thin films for high-density resistive switching memory. *Adv Mater*. 2019;31(49):1903679. doi:10.1002/adma.201903679

[43] Tian J, Zhang Y, Fan Z, et al. Nanoscale phase mixture and multifield-Induced topotactic phase transformation in $SrFeO_x$. *ACS Appl Mater Interfaces*. 2020;12(19):21883-21893. doi:10.1021/acsami.0c03684

[44] Lim E, Ismail R. Conduction mechanism of valence change resistive switching memory: a survey. *Electronics*. 2015;4(3):586-613. doi:10.3390/electronics4030586

[45] Li Z, Wang Y, Tian G, et al. High-density array of ferroelectric nanodots with robust and reversibly switchable topological domain states. *Sci Adv*. 2017;3(8):1700919. doi:10.1126/sciadv.1700919

[46] Yang W, Tian G, Fan H, et al. Nonvolatile ferroelectric-domain-wall memory embedded in a complex topological domain structure. *Adv Mater*. 2022;34(10):2107711. doi:10.1002/adma.202107711

[47] a) Li F, Zhang S, Damjanovic D, Chen L-Q, Shrout TR. Local structural heterogeneity and electromechanical responses of ferroelectrics: learning from relaxor ferroelectrics. *Adv Funct Mater*. 2018;28(37):1801504. doi:10.1002/adfm.201801504; b) Li F, Lin D, Chen Z, et al. Ultrahigh piezoelectricity in ferroelectric ceramics by design. *Nat Mater*. 2018;17(4):349-354. doi:10.1038/s41563-018-0034-4; c) Li F, Cabral MJ, Xu B, et al. Giant piezoelectricity of Sm-doped Pb($Mg_{1/3}Nb_{2/3}$)O_3-$PbTiO_3$ single crystals. *Science*. 2019;364(6437):264-268. doi:10.1126/science.aaw2781; d) Li F, Zhang S, Yang T, et al. The origin of ultrahigh piezoelectricity in relaxor-ferroelectric solid solution crystals. *Nat Commun*. 2016;7:13807. doi:10.1038/ncomms13807, https://www.nature.com/articles/ncomms13807#supplementary-information

[48] Liu Q, Zhang Y, Gao J, et al. High-performance lead-free piezoelectrics with local structural heterogeneity. *Energy Environ Sci*. 2018;11(12):3531-3539. doi:10.1039/C8EE02758G

[49] Takenaka H, Grinberg I, Liu S, Rappe AM. Slush-like polar structures in single-crystal relaxors. *Nature*. 2017;546(7658):391-395. doi:10.1038/nature22068

[50] a) Wu H, Zhang Y, Ning S, Zhao L-D, Pennycook SJ. Seeing atomic-scale structural origins and foreseeing new pathways to improved thermoelectric materials. *Materials Horizons*. 2019;6(8):1548-1570. doi:10.1039/C9MH00543A; b) He W, Wang D, Wu H, et al. High thermoelectric performance in low-cost $SnS_{0.91}Se_{0.09}$ crystals. *Science*. 2019;365(6460):1418-1424. doi:10.1126/science.aax5123; c) Qin B, Wang D, He W, et al. Realizing high thermoelectric performance in p-type SnSe through crystal structure modification. *J Am Chem Soc*. 2019;141(2):1141-1149. doi:10.1021/jacs.8b12450

[51] Zhao W, Liu Z, Sun Z, et al. Superparamagnetic enhancement of thermoelectric performance. *Nature*. 2017;549(7671):247-251. doi:10.1038/nature23667

[52] a) Xiao Y, Wu H, Li W, et al. Remarkable roles of Cu to synergistically optimize phonon and carrier transport in n-type PbTe-Cu_2Te. *J Am Chem Soc*. 2017;139(51):18732-18738. doi:10.1021/jacs.7b11662; b) Guo F, Cui B, Liu Y, et al. Thermoelectric SnTe with band convergence, dense dislocations, and interstitials through Sn self-compensation and mn alloying. *Small*. 2018;14(37):1802615. doi:10.1002/smll.201802615; c) Qin H, Sun S, Liu Y, et al. Constructing multi-type defects in $In_{0.1}Sb_{1.9}Te_3$-(MgB_2) composites: simultaneously enhancing the thermoelectric and mechanical properties. *Nano Energy*. 2021;90:106530. doi:10.1016/j.nanoen.2021.106530; d) Xiao Y, Wu H, Cui J, et al. Realizing high performance n-type PbTe by synergistically optimizing effective mass and carrier mobility and suppressing bipolar thermal conductivity. *Energy Environ Sci*. 2018;11(9):2486-2495. doi:10.1039/C8EE01151F; e) Xiao Y, Wu H, Wang D, et al. Amphoteric indium enables carrier engineering to enhance the power factor and thermoelectric performance in *n*-type $Ag_nPb_{100}In_nTe_{100+2n}$ (LIST. *Adv Energy Mater*. 2019;9(17):1900414. doi:10.1002/aenm.201900414; f) Qian X, Wu H, Wang D, et al. Synergistically optimizing interdependent thermoelectric parameters of *n*-type PbSe through alloying CdSe. *Energy Environ Sci*. 2019;12(6):1969-1978. doi:10.1039/C8EE03386B; g) Qian X, Wu H, Wang D, et al. Synergistically optimizing interdependent thermoelectric parameters of n-type PbSe through introducing a small amount of zn. *Materials Today Physics*. 2019;9:100102. doi:10.1016/j.mtphys.2019.100102; h) Xiao Y, Wang D, Zhang Y, et al. Band sharpening and band alignment enable high quality factor to enhance

thermoelectric performance in *n*-type PbS. *J Am Chem Soc*. 2020;142(8):4051-4060. doi:10.1021/jacs.0c00306; i) Qin H, Zhu J, Li N, et al. Enhanced mechanical and thermoelectric properties enabled by hierarchical structure in medium-temperature Sb_2Te_3 based alloys. *Nano Energy*. 2020;78:105228. doi:10.1016/j.nanoen.2020.105228

[53] Qin B, Zhang Y, Wang D, et al. Ultrahigh average ZT realized in p-type SnSe crystalline thermoelectrics through producing extrinsic vacancies. *J Am Chem Soc*. 2020;142(12):5901-5909. doi:10.1021/jacs.0c01726

[54] Yang D, Su X, Li J, et al. Blocking ion migration stabilizes the high thermoelectric performance in Cu_2Se composites. *Adv Mater*. 2020;32(40):2003730. doi:10.1002/adma.202003730

[55] a) Banik A, Ghosh T, Arora R, et al. Engineering ferroelectric instability to achieve ultralow thermal conductivity and high thermoelectric performance in $Sn_{1-x}Ge_xTe$. *Energy Environ Sci*. 2019;12(2):589-595. doi:10.1039/C8EE03162B; b) Sarkar D, Ghosh T, Roychowdhury S, et al. Ferroelectric instability induced ultralow thermal conductivity and high thermoelectric performance in Rhombohedralp-Type GeSe crystal. *J Am Chem Soc*. 2020;142(28):12237-12244. doi:10.1021/jacs.0c03696; c) Aggarwal L, Banik A, Anand S, Waghmare UV, Biswas K, Sheet G. Local ferroelectricity in thermoelectric SnTe above room temperature driven by competing phonon instabilities and soft resonant bonding. *J Materiomics*. 2016;2(2):196-202. doi:10.1016/j.jmat.2016.04.001

[56] a) Pei Y-L, Wu H, Wu D, Zheng F, He J. High thermoelectric performance realized in a BiCuSeO system by improving carrier mobility through 3D modulation doping. *J Am Chem Soc*. 2014;136(39):13902-13908. doi:10.1021/ja507945h; b) Wu D, Pei Y, Wang Z, et al. Significantly enhanced thermoelectric performance in n-type heterogeneous BiAgSeS composites. *Adv Funct Mater*. 2014;24(48):7763-7771. doi:10.1002/adfm.201402211

[57] Pei Y-L, Wu H, Sui J, et al. High thermoelectric performance in n-type BiAgSeS due to intrinsically low thermal conductivity. *Energy Environ Sci*. 2013;6(6):1750. doi:10.1039/c3ee40879e

[58] Wang D, Huang Z, Zhang Y, et al. Extremely low thermal conductivity from bismuth selenohalides with 1D soft crystal structure. *Sci Chin Mater*. 2020;63(9):1759-1768. doi:10.1007/s40843-020-1407-x

[59] a) Zhou Y, Wu H, Wang D, et al. Investigations on electrical and thermal transport properties of Cu_2SnSe_3 with unusual coexisting nanophases. *Mater Today Phys*. 2018;7:77-88. doi:10.1016/j.mtphys.2018.11.001; b) Wu HJ, Zhao LD, Zheng FS, et al. Broad temperature plateau for thermoelectric figure of merit ZT > 2 in phase-separated $PbTe_{0.7}S_{0.3}$. *Nat Commun*. 2014;5(1):4515. doi:10.1038/ncomms5515

[60] a) Xin J, Wu H, Liu X, Zhu T, Yu G, Zhao X. Mg vacancy and dislocation strains as strong phonon scatterers in $Mg_2Si_{1-x}Sb_x$ thermoelectric materials. *Nano Energy*. 2017;34:428-436. doi:10.1016/j.nanoen.2017.03.012; b) Liu Z, Meng X, Qin D, et al. New insights into the role of dislocation engineering in n-type filled skutterudite $CoSb_3$. *J Mater Chem C*. 2019;7(43):13622-13631. doi:10.1039/C9TC03839F; c) Qiu J, Luo T, Yan Y, et al. Enhancing the thermoelectric and mechanical properties of $Bi_{0.5}Sb_{1.5}Te_3$ modulated by the texture and dense dislocation networks. *ACS Appl Mater Interfaces*. 2021;13(49):58974-58981. doi:10.1021/acsami.1c19172; d) Hu L, Zhang Y, Wu H, et al. Entropy engineering of SnTe: multi-principal-element alloying leading to ultralow lattice thermal conductivity and state-of-the-art thermoelectric performance. *Adv Energy Mater*. 2018;8(29):1802116. doi:10.1002/aenm.201802116; e) Hu L, Zhang Y, Wu H, et al. Synergistic compositional–mechanical–thermal effects leading to a record high zT in n-type V_2VI_3 Alloys through progressive hot deformation. *Adv Funct Mater*. 2018;28(35):1803617. doi:10.1002/adfm.201803617; f) Guo F, Wu H, Zhu J, et al. Synergistic boost of output power density and efficiency in In-Li–codoped SnTe. *Proc Natl Acad Sci USA*. 2019;116(44):21998-22003. doi:10.1073/pnas.1911085116

[61] Zhao W, Liu Z, Wei P, et al. Magnetoelectric interaction and transport behaviours in magnetic nanocomposite thermoelectric materials. *Nat Nanotechnol*. 2017;12(1):55-60. doi:10.1038/nnano.2016.182

[62] Boona SR. Nanomagnets boost thermoelectric output. *Nature*. 2017;549(7671):169-170. doi:10.1038/549169a

[63] Jeen H, Choi WS, Biegalski MD, et al. Reversible redox reactions in an epitaxially stabilized SrCoO(x) oxygen sponge. *Nat Mater*. 2013;12(11):1057-1063. doi:10.1038/nmat3736

[64] Lu N, Zhang P, Zhang Q, et al. Electric-field control of tri-state phase transformation with a selective dual-ion switch. *Nature*. 2017;546(7656):124-128. doi:10.1038/nature22389

AUTHOR BIOGRAPHIES

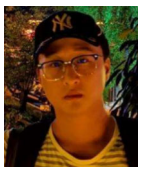

Guyang Peng received his BE from the Wuhan University of Technology in 2021. He is currently a master's student in Prof. Haijun Wu's group. His research interests include ferroelectric and piezoelectric materials and their microstructure characterization.

Haijun Wu is a professor at Xi'an Jiaotong University. He received his PhD in 2019, Prof. Pennycook's group, at the National University of Singapore, and then he finished his postdoctoral research in Prof. Pennycook's group. His research mainly focuses on the structural design, mechanism analysis, and performance regulation of ferroelectric, piezoelectric, and thermoelectric materials that can realize force-thermal-electric environment sensing and energy conversion.

Stephen J. Pennycook obtained his BA degree in natural sciences from the University of Cambridge, England, in 1975, and his MA and PhD degrees in physics from the same institution in 1978. He then continued at the University of Cambridge Cavendish Laboratory in postdoctoral positions until moving to the ORNL Solid State Division in 1982, where

he is now the leader of the Electron Microscopy Group. His main research interest is the study of materials through the technique of Z-contrast scanning transmission electron microscopy (STEM).

Xiangdong Ding is a professor at Xi'an Jiaotong University. He received his PhD in 1999, at the Jilin University, and then he finished his postdoctoral research at Xi'an Jiaotong University. His current research is focused on the phase transition behavior of ferro intelligent materials, deformation behavior of materials under extreme conditions, and new functional materials developed by strain engineering and domain boundary engineering.

How to cite this article: Peng G, Hu L, Qu W, et al. Structural-functional unit ordering for high-performance electron-correlated materials. *Interdiscip Mater*. 2022;1-23. doi:10.1002/idm2.12058